bioRxiv preprint doi: https://doi.org/10.1101/2020.02.21.959593; this version posted April 9, 2020. The copyright holder for this preprint (which was not certified by peer review) is the author/funder, who has granted bioRxiv a license to display the preprint in perpetuity. It is made available under aCC-BY-NC-ND 4.0 International license.

Title: FTO intronic SNP strongly influences human neck adipocyte browning determined by tissue and PPARγ specific regulation: a transcriptome analysis

Beáta B. Tóth[a], Rini Arianti[a,b], Abhirup Shaw[a,b], Attila Vámos[a,b], Zoltán Veréb[c,d], Szilárd Póliska[a], Ferenc Győry[e], Zsolt Bacso[f], László Fésüs[a,], Endre Kristóf[a,*]*

László Fésüs and Endre Kristóf contributed equally to this work.

[a]Department of Biochemistry and Molecular Biology, Faculty of Medicine, University of Debrecen, Debrecen, Hungary; H-4032, Debrecen, Egyetem Tér 1., Hungary
[b]Doctoral School of Molecular Cell and Immune Biology, University of Debrecen, Debrecen, Hungary; H-4032, Debrecen, Egyetem tér 1., Hungary
[c]Regenerative Medicine and Cellular Pharmacology Research Laboratory, Department of Dermatology and Allergology, University of Szeged, Szeged, Hungary; H-6720, Szeged, Korányi fasor 6., Hungary
[d]HCEMM-SZTE Skin Research Group, University of Szeged, Szeged, Hungary
[e]Department of Surgery, Faculty of Medicine, University of Debrecen, Debrecen, Hungary; H-4032, Debrecen, Móricz Zsigmond körút 22., Hungary
[f]Department of Biophysics and Cell Biology, Faculties of Medicine and Pharmacology, University of Debrecen, Debrecen, Hungary; H-4032, Debrecen, Egyetem Tér 1., Hungary

[*]Corresponding authors:

László Fésüs, MD PhD DSc MHASc
Department of Biochemistry and Molecular Biology
Faculty of Medicine
University of Debrecen
H-4032, Debrecen, Egyetem Tér 1., Hungary
Tel: +3652-416-432, Fax: +3652-314-989
E mail: fesus@med.unideb.hu

Endre Kristóf, MD PhD
Department of Biochemistry and Molecular Biology
Faculty of Medicine
University of Debrecen
H-4032, Debrecen, Egyetem Tér 1., Hungary
Tel: +3652-416-432, Fax: +3652-314-989
E mail: kristof.endre@med.unideb.hu

Declarations of interest: none

bioRxiv preprint doi: https://doi.org/10.1101/2020.02.21.959593; this version posted April 9, 2020. The copyright holder for this preprint (which was not certified by peer review) is the author/funder, who has granted bioRxiv a license to display the preprint in perpetuity. It is made available under aCC-BY-NC-ND 4.0 International license.

Abbreviations

adenosine triphosphate: ATP
analysis of variance: ANOVA
body mass index: BMI
bone morphogenetic protein: BMP
brown adipose tissue: BAT
carnitine palmitoyltransferase: CPT
cell death-inducing DFFA-like effector A: CIDEA
creatine kinase, mitochondrial: CKMT
3',5'-cyclic adenosine monophosphate: cAMP
cytosine: C
deep neck: DN
differentially expressed gene: DEG
extracellular acidification rate: ECAR
extracellular matrix: ECM
fat mass and obesity-associated: FTO
human adipose-derived stromal cells: hASC
interleukin: IL
Kruppel-like factor 11: KLF11
oxygen consumption: OC
oxygen consumption rate: OCR
peptidase M20 domain containing 1: PM20D1
peroxisome proliferator-activated receptor gamma: PPARγ
polymerase chain reaction: PCR
single nucleotide polymorphism: SNP
subcutaneous: SC
thymine: T
T-Box 1: TBX1
uncoupling protein 1: UCP1
Zic family member 1: ZIC1

bioRxiv preprint doi: https://doi.org/10.1101/2020.02.21.959593; this version posted April 9, 2020. The copyright holder for this preprint (which was not certified by peer review) is the author/funder, who has granted bioRxiv a license to display the preprint in perpetuity. It is made available under aCC-BY-NC-ND 4.0 International license.

Abstract

Brown adipocytes, abundant in deep-neck (DN) area in humans, are thermogenic with anti-obesity potential. FTO pro-obesity rs1421085 T-to-C SNP shifts differentiation program towards white adipocytes in subcutaneous fat. Human adipose-derived stromal cells were obtained from subcutaneous neck (SC) and DN fat of 9 donors, of which 3-3 carried risk-free (T/T), heterozygous or obesity-risk (C/C) FTO genotypes. They were differentiated to white and brown (long-term PPARγ stimulation) adipocytes, then global RNA sequencing was performed and differentially expressed genes (DEGs) were compared. DN and SC progenitors had similar adipocyte differentiation potential but differed in DEGs. DN adipocytes displayed higher browning features according to ProFAT or BATLAS scores and characteristic DEG patterns revealing associated pathways which were highly expressed (thermogenesis, interferon, cytokine, retinoic acid, with UCP1 and BMP4 as prominent network stabilizers) or downregulated (particularly extracellular matrix remodelling) compared to SC ones. Part of DEGs in either DN or SC browning was PPARγ-dependent. Presence of the FTO obesity-risk allele suppressed the expression of mitochondrial and thermogenesis genes with a striking resemblance between affected pathways and those appearing in ProFAT and BATLAS, underlining the importance of metabolic and mitochondrial pathways in thermogenesis. Among overlapping regulatory influences which determine browning and thermogenic potential of neck adipocytes, FTO genetic background has a so far not recognized prominence.

Keywords: adipocyte browning, differential gene expression patterns, deep-neck, PPARγ, FTO obesity-risk allele

bioRxiv preprint doi: https://doi.org/10.1101/2020.02.21.959593; this version posted April 9, 2020. The copyright holder for this preprint (which was not certified by peer review) is the author/funder, who has granted bioRxiv a license to display the preprint in perpetuity. It is made available under aCC-BY-NC-ND 4.0 International license.

1. INTRODUCTION

Brown and beige adipocytes play a major role in maintaining the constant core body temperature of hibernating, small and newborn animals, as well as in humans without shivering [1,2]. Their heat production is mainly mediated by UCP1, a mitochondrial carrier protein, which uncouples ATP synthesis from the respiratory chain activity [1,3]. These adipocytes also conduct effective UCP1-independent thermogenic mechanisms [4-9]. The stimulation of these processes leads to increased energy expenditure that can ameliorate the energy balance during obesity and type 2 diabetes mellitus [10,11].

In rodents, brown adipose tissue (BAT) contains classical brown adipocytes which derive from myogenic precursors, accumulate numerous small lipid droplets in a multilocular arrangement and convert glucose and fatty acids into heat mostly by the action of the constitutively expressed UCP1 [1,2,12]. Beige adipocytes with similar morphologic features were also described in mice. These cells arise from mesenchymal precursors and have a common developmental origin with white adipocytes, exist in distinct thermogenic fat depots and can be induced by cold and subsequent adrenergic stimulation [2,13]. In adult humans specific adipose depots are enriched in brown adipocytes; these expanse to 1-1.5% of total body mass and are mostly found in the perirenal, deep-neck (DN) and paravertebral regions [14]. It is still unrevealed whether these thermogenic fat depots represent the classical brown or the beige type of adipocytes by origin and function, even after recent intense studies of DN tissue which could be compared to paired subcutaneous (SC) fat samples [15-18]. For simplicity, in this paper, the term brown is used to cover both classical and beige thermogenic adipocytes in humans.

Human brown adipocytes differentiated in distinct adipose tissues express thermogenic genes at moderate levels under unstimulated conditions [2,14]. The ratio of brown and white adipocytes is partially determined during the early differentiation of mesenchymal progenitors into adipocyte subtypes which is strongly influenced by genetic predisposition [19,20]. This can be quantified in a given tissue or cell culture sample by determining BATLAS score based on the expression of 98 brown and 21 white-specific genes, which were selected by a combined analysis of gene expression signatures in murine brown, beige and white adipocytes and human tissue samples [21]. Similarly, browning probability can be estimated by a recently developed computational tool, ProFAT [22].

A recent genome-wide association study of body fat distribution identified 98 independent adiposity loci which could affect the appearance of thermogenic fat [23]. In a detailed study by Claussnitzer et al. it has been described that single nucleotide polymorphism (SNP) rs1421085 underlies the genetic association between fat mass and obesity-associated (FTO) locus; obesity and the presence of the C risk-allele of the FTO locus results in a cell-autonomous, IRX3 and IRX5 dependent shift in the gene expression programs, generating white adipocytes instead of brown with lipid-storage and decreased thermogenesis. When the T/T risk-free genotype is carried at the rs1421085 position, the ARIDB5 repressor becomes able to bind to this site not allowing IRX3 and 5 expressions which let adipocyte precursors to be committed for brown differentiation [19].

To learn more about human adipocyte browning and attempting to through more light on unresolved or controversial issues in the regulation of thermogenesis, we decided to study neck adipocyte populations derived from primary human adipose-derived stromal cells (hASCs) instead of whole tissue samples with different cell types present or single-cell clones

bioRxiv preprint doi: https://doi.org/10.1101/2020.02.21.959593; this version posted April 9, 2020. The copyright holder for this preprint (which was not certified by peer review) is the author/funder, who has granted bioRxiv a license to display the preprint in perpetuity. It is made available under aCC-BY-NC-ND 4.0 International license.

influenced by immortalization protocols. We screened and compared global gene expression patterns by RNA sequencing of hASC-derived white and brown (in response to sustained PPARγ stimulation) differentiated adipocytes. The hASCs were isolated from paired DN and SC adipose tissue samples of nine donors, 3 of each FTO rs1421085 genotype: T/T-risk-free, T/C-heterozygous, C/C-obesity-risk. We found that both brown and beige markers, including *UCP1*, *CKMT1A/B* [4,15], *CIDEA* [24], or *PM20D1* [6] were upregulated in DN as compared to SC adipocytes, indicating a large potential of thermogenesis in the deep depots. Novel pathways and biological processes could be linked to browning regulation comparing patterns of upregulated genes and disentangling the complicated set of interactions at protein level which may point out the most indispensable proteins need to maintain the particular phenotype. On the other hand, dozens of genes (such as *CIDEA*, *CITED1* [25] or *PM20D1* thermogenic markers) were upregulated in response to the brown differentiation as compared to white irrespective of the anatomical origin of the hASCs. The gene expression pattern of brown adipocytes was determined to a greater extent by the anatomical origin of the hASCs from which they had been differentiated than the differentiation protocol. Surprisingly, the expression of metabolic, mitochondrial and thermogenic genes was strikingly compromised by the presence of FTO rs1421085 genotypes in the progenitors. Our results suggest that cultivated hASCs from distinct locations of the human neck still keep their differing propensity for adipocyte browning which is strongly influenced by the presence of the obesity-risk alleles at the FTO intronic locus.

bioRxiv preprint doi: https://doi.org/10.1101/2020.02.21.959593; this version posted April 9, 2020. The copyright holder for this preprint (which was not certified by peer review) is the author/funder, who has granted bioRxiv a license to display the preprint in perpetuity. It is made available under aCC-BY-NC-ND 4.0 International license.

2. MATERIALS AND METHODS

2.1 Ethics statement and obtained samples, isolation and differentiation of hASCs

Tissue collection was complied with the guidelines of the Helsinki Declaration and was approved by the Medical Research Council of Hungary (20571-2/2017/EKU) followed by the EU Member States' Directive 2004/23/EC on presumed consent practice for tissue collection. Written informed consent was obtained from all participants before the surgical procedure. hASCs were isolated from SC and DN adipose tissue of volunteers (BMI<29.9) aged 35–75 years after written informed consent. During thyroid surgeries a pair of DN and SC adipose tissue samples was obtained to rule out inter-individual variations. Patients with known diabetes, malignant tumor or with abnormal thyroid hormone levels at the time of surgery were excluded [26].

hASCs were isolated and cultivated; white and brown adipocytes were differentiated from hASCs according to described protocols [6,7,26,27]. Briefly, both white and brown differentiations were induced by hormonal cocktails in serum and additive-free DMEM-F12-HAM medium that contain apo-transferrin (Sigma-Aldrich cat#T2252), insulin (Sigma-Aldrich cat#I9278), T3 (Sigma-Aldrich cat#T6397), dexamethasone (Sigma-Aldrich cat#D1756), and IBMX (Sigma-Aldrich cat#I5879). Later, dexamethasone and IBMX were omitted from both media. In the white cocktail hydrocortisone (Sigma-Aldrich cat#H0888) was constantly present, while the brown contained insulin at 40x higher concentration than the white. However, the major difference between the two protocols was the time interval and concentration of the administered rosiglitazone (Cayman Chemicals cat#71740). While the white regimen contained 2 µM rosiglitazone on the first four days of the two weeks long process, the differentiating brown adipocytes were treated with the drug at 500 nM concentration between the 4th and 14th days [28,29]. The absence of mycoplasma was checked by polymerase chain reaction (PCR) analysis (PCR Mycoplasma Test Kit I/C, PromoCell cat# PK-CA91) [7,26].

2.2 Flow cytometry

To investigate the phenotype of the undifferentiated hASCs, multiparametric analysis of surface antigen expression was performed by three-color flow cytometry using fluorochrome-conjugated antibodies with isotype matching controls. See references 7 and 30 for further details about the analysis.

2.3 RNA and DNA isolation, genotyping

RNA and DNA preparation was carried out as described previously [6,7,26,27]. Rs1421085 SNP was genotyped by qPCR using TaqMan SNP Genotyping assay (Thermo Scientific cat#4351379) according to the Manufacturer's instructions [7].

2.4 RNA-Sequencing

To obtain global transcriptome data, high throughput mRNA sequencing analysis was performed on Illumina sequencing platform. Total RNA sample quality was checked on Agilent BioAnalyzer using Eukaryotic Total RNA Nano Kit according to the Manufacturer's protocol. Samples with RNA integrity number (RIN) value >7 were accepted for the library preparation process. Libraries were prepared from total RNA using NEBNext® Ultra™ II

bioRxiv preprint doi: https://doi.org/10.1101/2020.02.21.959593; this version posted April 9, 2020. The copyright holder for this preprint (which was not certified by peer review) is the author/funder, who has granted bioRxiv a license to display the preprint in perpetuity. It is made available under aCC-BY-NC-ND 4.0 International license.

RNA Library Prep for Illumina (New England BioLabs, Ipswich, MA, USA) according to the manufacturer's protocol. Briefly, poly-A RNAs were captured by oligo-dT conjugated magnetic beads then the mRNAs were eluted and fragmented at 940C degree. First-strand cDNA was generated by random priming reverse transcription and after second strand synthesis step, double-stranded cDNA was generated. After repairing ends, A-tailing and adapter ligation steps, adapter-ligated fragments were amplified in enrichment PCR and finally sequencing libraries were generated. Sequencing runs were executed on Illumina NextSeq500 instrument using single-end 75 cycles sequencing.

After sequencing, the reads were aligned to the GRCh38 reference genome (with EnsEMBL 95 annotation) using STAR aligner (version 2.7.0a) [31]. To quantify our reads to genes, featureCounts was used (version: 1.6.3) [32].

Subsequent gene expression analyses were performed in R (version 3.5.2). Genes with low expression values or with outlier value were removed from further analysis. Briefly, after removing the highest read value of each gene we filtered out genes with reads was less than 50 considering raw reads count. Then, to further remove outlier genes we calculated Cook's distance and filtered out genes with Cook's distance higher than 1. After filtering out the low-expressed and outlier ones, the expression profile of 22362 transcripts could be examined. PCA analysis did not show any batch effect, considering sequencing date, the donor origin, and the donor sex or tissue origin. Differential expression analysis was performed using DESeq2 algorithm (version 1.22.2). When tissue origin and differentiation protocol based differential expression was determined donor origin was controlled to decrease the effect of biological variance on thermogenic capacity [33]. However, when the comparison was based on the FTO obesity-risk allele presence, we did not control donor origin. Significantly differentially expressed genes (DEGs) were defined based on adjusted P values <0.05 and log2 fold change threshold >0.85.

Hierarchical cluster analyses and heat map visualization was performed on the Morpheus web tool (https://software.broadinstitute.org/morpheus/) using Pearson correlation of rows and columns and complete linkage based on calculated z-score of DESeq normalized data after log2 transformation. The z-score was calculated in two ways: to eliminate the donor background we calculated it by donors, or to examining FTO obesity-risk allele presence-based donor differences we determined it by considering all samples, as indicated at the figures. The interaction network and significantly enriched pathways (Reactome and KEGG or Biological processes) were determined by STRING (https://string-db.org). Edges represent protein-protein interactions. To identify Interaction network we took consideration of text mining, databases and experiments from the active interaction source from the STRING database and interaction strength score threshold was 0.4. Further analyzes of the STRING network data was performed in igraph R to identify betweenness score and bridges numbers of the interacting nodes. Different interaction thresholds (0.4-0.7) were used to visualize the network, as indicated in the figures, to obtain the interpretable complexity of the network. Interactomes were also constructed by Gephi which visualizes the fold change of the genes. Prediction of browning capacity was performed using PROFAT (http://ido.helmholtz-muenchen.de/profat/) and BATLAS (http://green-l-12.ethz.ch:3838//BATLAS/) computational tools.

RNAseq data have been deposited to Sequence Read Archive (SRA) database (https://www.ncbi.nlm.nih.gov/sra) under accession number PRJNA607438.

bioRxiv preprint doi: https://doi.org/10.1101/2020.02.21.959593; this version posted April 9, 2020. The copyright holder for this preprint (which was not certified by peer review) is the author/funder, who has granted bioRxiv a license to display the preprint in perpetuity. It is made available under aCC-BY-NC-ND 4.0 International license.

2.5 Antibodies and immunoblotting

Lysis of differentiated adipocytes, denaturation, SDS-PAGE and blotting were performed as described previously. For overnight, membranes were probed at 4ºC with primary antibodies: polyclonal anti-UCP1 (1:500, Sigma-Aldrich cat#U6382), and anti-actin (1:10000, Sigma-Aldrich cat#A2066) in TBS-T containing 1 % non-fat skimmed milk, followed by the incubation with horseradish-peroxidase-conjugated anti-rabbit secondary antibody (Sigma-Aldrich Cat#A1949) for 1 hour at room temperature. Immunoreactive proteins were visualized by Immobilion western chemiluminescence substrate (Merck-Millipore cat#WBKLS0500) [7].

2.6 Immunofluorescence staining, quantification of browning

hASCs were plated and differentiated on Ibidi eight-well μ-slides; vital and immunofluorescence staining was carried out as described previously [6,7,26,27]. Sample scanning was done by iCys Research Imaging Cytometer (iCys, Thorlabs Imaging Systems, Sterling, VA, USA). The images were processed and analyzed by our high-throughput automatic cell-recognition protocol using the iCys companion software (iNovator Application Development Toolkit version 7.0, CompuCyte Corporation, Westwood, MA, USA), Cell Profiler and Cell Profiler Analyst (The Broad Institute of MIT, MA, USA). Texture sum variance and median Ucp1 protein content of adipocytes (as compared to SC white adipocytes) per cell was determined. In every experiment, 2000 cells per each sample were recorded and measured. See references 7, 27 and 34 for further details about the analysis.

2.7 Determination of cellular oxygen consumption (OC) and extracellular acidification rate (ECAR)

OC and ECAR were measured using an XF96 oxymeter (Seahorse Biosciences, North Billerica, MA, USA). hASCs of donors not related to the RNA-Seq analysis were seeded and differentiated in 96-well XF96 assay plates. Baseline, dibutyril-cAMP (Sigma-Aldrich cat#D0627) stimulated, β-guanidinopropionic acid (Sigma-Aldrich cat#G6878) and oligomycin (Enzo Life Sciences cat#ALX-380-037) inhibited OC and ECAR were recorded. As the last step, cells received a single bolus dose of Antimycin A (Sigma-Aldrich cat# U8674) at 10 μM final concentration for baseline correction. The oxygen consumption rate (OCR) and ECAR were normalized to protein content and normalized readings were shown. For statistical analysis, relative OC and ECAR levels were determined to compare basal, cAMP stimulated and oligomycin inhibited (both in unstimulated and stimulated cells) OCRs/ECARs of each sample to the basal OCR/ECAR of untreated SC white adipocytes [6,7,26].

2.8. Statistical analysis

Results are expressed as the mean±s.d. for the number of donors indicated. The normality of distribution of the data was tested by Shapiro–Wilk test. In a comparison of two groups, two-tailed Student's t-test was used. For multiple comparisons of groups statistical significance was calculated and evaluated by two-way ANOVA followed by Tukey post-hoc test. Statistical analysis of differential expression was performed in the R programing language with DESeq [35]. Hierarchical cluster analysis during heat map generation was performed based on Pearson correlation. n values represent biological replicates. Specific details for n value are noted in each figure legend.

bioRxiv preprint doi: https://doi.org/10.1101/2020.02.21.959593; this version posted April 9, 2020. The copyright holder for this preprint (which was not certified by peer review) is the author/funder, who has granted bioRxiv a license to display the preprint in perpetuity. It is made available under aCC-BY-NC-ND 4.0 International license.

3. RESULTS

3.1 DN and SC progenitors have similar surface markers and adipocyte differentiation potential but differ in the gene expression profile

We intended to examine global gene expression patterns of hASC-derived white and brown adipocytes and undifferentiated progenitors cultivated from paired DN and SC adipose tissue biopsies. Before doing that, we aimed to validate if adipocytes differentiated for two weeks from the aforementioned hASCs isolated from four individuals have different functional properties as described in previous studies [18,36]. Basal and proton leak mitochondrial respiration of DN adipocytes was significantly elevated as compared to the SC adipocytes regardless of the obtained protocol **(Supplementary Figure S1A)**. After the cells received a single bolus dose of cell-permeable dibutyril-cAMP, mimicking adrenergic stimulation, we found that adipocytes which were differentiated from DN precursors were more capable to activate their respiration than the adipocytes of SC origin. In parallel, basal and cAMP-stimulated extracellular acidification rates of DN adipocytes were greater in a significant degree than those of the SC ones **(Supplementary Figure S1B)**. We could also estimate, by applying the creatine analogue β-GPA, the contribution of UCP1-independent creatine futile cycle to oxygen consumption [4] and found it was more pronounced in DN adipocytes **(Supplementary Figure S1C)**.

As a further characterization of the hASCs, surface antigen analysis was performed. There was no significant difference in the presence of hematopoietic/monocyte, fibroblast, endothelial and integrin cell surface markers between the SC and DN precursors **(Figure 1A** and **Supplementary Table S1)**. Less than 5% of them had CD31, CD45 and CD146 markers which exclude substantial endothelial or leukocyte contamination. Primary abdominal subcutaneous hASCs and SGBS cells which also can be differentiated to both white and brown adipocytes [7,27,34] differed in the presence of the MCAM marker CD146.

Comparing the global gene expression profile of the hASCs obtained from the two anatomical sites of nine donors, large differences were observed. Numbers 1 to 9 on corresponding figures throughout the manuscript label individual donors from whom the samples were obtained. In this comparison, 1420 genes were differentially expressed: 878 were higher in DN and 542 in SC progenitors, respectively **(Figure 1B)**. The list of significantly enriched pathways (only 10 are shown), determined by considering the higher expressed genes, is very different between the two progenitors, except the similarly high expression of genes related to extracellular matrix (ECM) regulation. The DN hASC profile was dominated by the complement and coagulation cascade, retinoic acid biosynthesis and signaling, interaction between L1 and ankyrins, and neuronal systems and hemostasis pathways. SC precursors showed characteristic enrichment for homeobox/homeodomain mediated transcription regulation, neuroactive ligand-receptor interaction, PPAR signaling, synthesis of GPI-anchor proteins, and integrin cell surface interaction pathways **(Figures 1C-F**; Italic fonts indicate enriched pathway, biological process or compounds which also appear in some comparisons of differentiated samples presented in other figures). Unexpectedly, low levels of *UCP1* expression were also detected in some preadipocyte samples, and this was more pronounced in SC preadipocytes.

The DN and SC hASCs isolated from the nine independent donors were differentiated and analyzed by laser-scanning cytometry [6,7,26,27]. The efficiency of their differentiation to adipocytes defined by expression of general fat cell markers did not differ significantly by the

bioRxiv preprint doi: https://doi.org/10.1101/2020.02.21.959593; this version posted April 9, 2020. The copyright holder for this preprint (which was not certified by peer review) is the author/funder, who has granted bioRxiv a license to display the preprint in perpetuity. It is made available under aCC-BY-NC-ND 4.0 International license.

site of origin or differentiation protocol **(Figure 2A)**. The most prominent adipogenic marker genes [37] **(Supplementary Table S2)** were expressed significantly higher (except *STAT3*) in all mature adipocyte samples as compared to progenitors and were not significantly different between SC and DN adipocytes or samples differentiated with white and brown protocols. Hierarchical cluster analysis of these genes confirmed that the samples clustered into two main groups according to their differentiation status but not by tissue origin or the differentiation protocol used, suggesting that these factors had no effect on the general adipocyte differentiation efficiency of the progenitor cells **(Figure 2B)**.

3.2 Differentiated adipocytes from DN progenitors display higher browning-related gene-expression features

Next, we investigated morphology and differential transcriptomic characteristics of adipocytes differentiated from hASCs of the nine donors. Laser-scanning cytometric data clearly showed that the DN adipocyte population, differentiated by either the white or the brown protocol, had more brown cells characterized by the appearance of UCP1 and small lipid droplets **(Figure 2C)**. To compare tissue origin and differentiation protocol-dependent transcriptional changes related to browning, recently developed computational tools ProFAT and BATLAS were applied. When the ProFAT browning gene-set [22] was used to score browning probability, browning markers were expressed higher in the DN samples irrespective of the differentiation protocol **(Figures 2D** and **E)** and appeared in distinct clusters **(Supplementary Figure S2)**. Expression of BATLAS genes visualized as heat map by hierarchical clustering **(Figure 2F)** also showed that the differentiated DN and SC samples predominantly appeared in these two main distinct clusters. Interestingly, even the white differentiation protocol resulted in BATLAS defined brown cell content **(Figure 2G)** while the highest brown cell percentage appeared in DN samples with noticeable donor variance (which was apparent in ProFAT scores as well). Six out of the BATLAS browning marker genes (*UCP1*, *CPT1B*, *EHHADH*, *AKAP1*, *SOD2*, and *ACSL5*) were expressed significantly higher in differentiated DN samples **(Supplementary Figure S3)**. Interestingly, the classical brown adipocyte marker *ZIC1* [16], was lowly expressed in both DN and SC adipocytes, and its expression was significantly increased only when the SC progenitor samples were differentiated by the brown protocol; this data questions the applicability of *ZIC1* as a lineage-specific, brown adipocyte marker gene.

Checking the expression of UCP1 at the protein level in differentiated adipocytes we detected the highest UCP1 content in brown adipocyte samples of DN origin **(Figure 2H)** while in adipocytes of SC origin the UCP1 expression was lower. Based on the above cytometric, gene expression and metabolic data it can be concluded that adipocytes differentiated from DN progenitors have greater thermogenic potential as compared to those originated from SC adipose tissue, suggesting that cultivated hASC of distinct anatomical locations maintain their different potentials for browning *ex vivo*.

3.3 Differential gene expression patterns reveal network pathways associated with higher browning potential of DN adipocytes

After establishing the higher browning potential of cell populations derived from DN, we examined the pattern of DEGs between the DN and SC samples. Considering both the white and the brown differentiation protocol, 1049 genes were expressed differentially in matured DN adipocytes. Approximately half of these genes were already differentially expressed at preadipocyte state (272 were higher and 250 lower expressed in DN), but the other half

bioRxiv preprint doi: https://doi.org/10.1101/2020.02.21.959593; this version posted April 9, 2020. The copyright holder for this preprint (which was not certified by peer review) is the author/funder, who has granted bioRxiv a license to display the preprint in perpetuity. It is made available under aCC-BY-NC-ND 4.0 International license.

became expressed differentially only in differentiated adipocytes (257 were higher and 270 lower expressed in DN adipocytes) **(Figures 3A** and **B)**. Relating the DEGs in mature adipocytes to how they were expressed in preadipocytes, four distinct groups could be defined. **Figure 3A** shows a global heat map representation of the expression profile in the four groups.

257 genes (Group 1) were expressed at a greater extent in differentiated DN adipocytes as compared to SC ones and this differential expression was not observed in DN versus SC preadipocytes **(Figures 1B** and **C)**. This group includes well-established browning marker genes such as *UCP1*, *PRDM16*, *CKMT1A/B*, *CIDEA*, and *PM20D1* **(Supplementary Figure S3)**. In further analyses, interaction relationships among products of higher expressed genes could be revealed using the STRING computational tool which also defined enriched pathways (KEGG and REACTOM), biological processes or cell compartments **(Figures 3C** and **D, Supplementary Figure S4A** by Gephi). Most of the browning marker genes mentioned above appeared in a separate cluster (black square). Interestingly, signaling pathways such as interferon alpha/beta, rhodopsin-like receptors, TRAF3-dependent IRF activation pathway and cytokine-cytokine receptor interactions were predominant among DN specific clusters, whereas metabolic pathways were scarce. These significantly enriched pathways were clearly linked to differentiated DN brown cells as they did not appear in DN preadipocytes as enriched pathways when compared to SCs **(Figures 1B-D)**. We then sought to find linkers among the characteristic functional modules of the DN specific interaction network which might have the most pronounced effect on the structure of the entire interactome. We calculated the betweenness centrality scores to point out important genes that connect different functional modules and the number of bridges to learn how many modules are connected by this gene. This network analysis confirmed the key role of *UCP1* to maintain network integrity. Other genes, such as *ESR1*, *MT2A*, *LEPR2*, *IRF7*, and *AGT* may be also pivotal for this network **(Table 1A)**.

272 genes (Group 2) were expressed at a greater extent in DN as compared to SC preadipocytes and their expression remained elevated in DN adipocytes as compared to SC ones after white or brown differentiation, presumably contributing to a higher propensity to browning **(Figures 3A** and **B)**. The most affected pathways were complement and coagulation cascades, signaling by retinoid acid and interaction between L1 and ankyrins **(Figures 3E** and **F, Supplementary Figure S4B** by Gephi). As expected, pathways in this group were already revealed in the analysis of higher expressed genes in DN versus SC preadipocytes **(Figures 1B-D**, Italic font: pathway also appears in preadipocyte state; Capital letters: Pathway also appears in FTO obesity-risk allele based comparison shown below). Similarly, expression of ECM and lipid metabolism genes is different in progenitors and this difference remains significant in mature adipocytes. Also, transcriptional regulation by Homeodomain/Homeobox containing transcriptional factors was tissue-specific and not affected by the differentiation state. The *BMP4* gene seems to be of paramount importance for a stable network structure; its role was already established for adipogenesis, promotion of adipocyte differentiation and brown fat development where it induces UCP1 expression [38]. In addition, *CD34*, *EFNA5*, *RARB* and *ALDH1A3* genes appeared, according to betweenness and bridges scores, to have importance in this interactome network **(Table 1B)**. *TBX1*, a well-established beige marker gene [17], also appeared in this group as an important network member.

bioRxiv preprint doi: https://doi.org/10.1101/2020.02.21.959593; this version posted April 9, 2020. The copyright holder for this preprint (which was not certified by peer review) is the author/funder, who has granted bioRxiv a license to display the preprint in perpetuity. It is made available under aCC-BY-NC-ND 4.0 International license.

3.4 Downregulated pathways in DN adipocytes

270 genes (Group 3) were downregulated in differentiated DN adipocytes compared to SCs and this differential expression was not seen in the preadipocyte state; expression of some of these genes may be non-permissive for browning. STRING network and pathway analysis showed that these genes were predominantly involved in remodeling of the ECM, cell adhesion and synthesis of GPI-anchored proteins pathways **(Figures 4A** and **B, Supplementary Figure S4C** by Gephi). Cytokine signaling was also highlighted as several interleukin receptors (e.g. *IL1RE*, *IL18RE*, *IL20RE*), *TGFB3* and *KIT* were expressed higher in the matured SC adipocytes **(Figures 4C** and **D)**. *COL1A1* plays a central role in the network, but *GPC3*, *KRT7*, *CNR1*, and *SEMA3A* are also important in sustaining a stable network structure **(Table 2A)**.

250 genes (Group 4) were expressed at a lower extent in DN preadipocytes as compared to SC and their expression remained low in the DN adipocytes as compared to SC ones after white or brown differentiation; these may be part of pathways which are not permissive for browning either. ECM organization pathways had outstanding dominance among the related pathways and the repeated appearance of the GPI-anchored protein pathway (SC preadipocytes and Group 3) emphasizes the importance of glycosylphosphatidylinositol-anchored membrane proteins in the formation of the SC phenotype. In addition, the transcription regulation by homeobox and homeodomain and the neuroactive ligand-receptor interaction pathways also appeared in this group **(Figures 4C** and **D, Supplementary Figure S4D** by Gephi). When analyzing relationships, *POSTN* was the most significant, but *RUNX2*, *NCAM1*, *GATA2*, *EDIL3*, and *PAX3* could be also important for maintaining network connectivity. Based on their network position, the *IRX1*, *IRX3*, and *GRIA3* expressed higher in SC adipocytes may have roles in restraining browning potential **(Table 2B)**.

3.5 Shared PPARγ mediated gene expression patterns in DN and SC adipocytes

Both ProFAT and BATLAS estimations clearly showed that SC precursor cells also reacted to browning as compared to the white differentiation protocol by upregulating brown genes. The degree of upregulation of these genes could be similar in DN and SC adipocytes and missed when DN and SC data were compared. Therefore, we analyzed genes which responded similarly to brown differentiation protocol that is long-term rosiglitazone exposure, in SC and DN adipocytes. Indeed, out of the 217 genes responding by upregulation to brown differentiation in either DN or SC adipocytes, only 40 **(Supplementary Table S3)** were also present in Groups 1 and 2 (529 genes) described above. Eighty genes were expressed higher in brown adipocytes irrespective to their anatomical origin and they displayed enrichment of the PPAR signaling pathway **(Figures 5A-C)**. Regarding the latter glycerol kinase, *PCK1*, *CPT1B* were present among BATLAS genes [21], PLIN5 was linked to browning [39], ANGPTL4 had not been investigated yet in this respect. In an earlier report Loft et al. claimed that browning of human adipocytes, induced by PPARγ stimulation by rosiglitazone of stem cells isolated from the prepubic fat pad of a 4-month-old male donor, required the metabolic regulator Kruppel-like factor 11 (KLF11) and reprogramming of a PPARγ super-enhancer [40]. We found that *KLF11* was among the rosiglitazone upregulated genes **(Figure 5D)** in either SC or DN adipocytes suggesting that it may be involved in the regulation of browning of neck area adipocytes.

Among the upregulated browning genes outside of the PPAR pathway, *CIDEA* was listed by ProFAT and also found in the Group 1 genes above, similarly to *PM20D1* which was strongly

bioRxiv preprint doi: https://doi.org/10.1101/2020.02.21.959593; this version posted April 9, 2020. The copyright holder for this preprint (which was not certified by peer review) is the author/funder, who has granted bioRxiv a license to display the preprint in perpetuity. It is made available under aCC-BY-NC-ND 4.0 International license.

influenced by natural genetic variations in humans [41] and *CPT1B* which was essential for beta-oxidation of fatty acids. Gamma-butyrobetaine dioxygenase (BBOX1) catalyzes the formation of L-carnitine from gamma-butyrobetaine and has been reported to play a role in adipocyte browning [42]. The beige marker *CITED1* is a transcriptional coactivator of the p300/CBP-mediated transcription complex [25]. Higher expression of glycerol phosphate acyltransferase (GPAT3) in SC and DN brown adipocytes reflects increased triacylglycerol synthesis capacity. The mitochondrial membrane transporter for long-chain fatty acids (SLC27A3) was also upregulated in response to PPARγ stimulation. There were several other highly upregulated genes (e.g. *OAS*, *CD96*, *KRT79*) which should be investigated in the future for their possible role in brown adipocyte function. Altogether, these data show that in addition to DN anatomical location browning potential is also influenced by the appearance of PPARγ ligands in both SC and DN adipocytes.

The browning protocol also downregulated a large number of genes in either DN or SC preadipocytes and 35 overlap with Groups 3 and 4 **(Supplementary Table S4)**. Out of the downregulated genes, 70 were downregulated in cells from both DN and SC origin with the indication of the importance of glutathione and arachidonic acid metabolism pathways **(Figures 5E** and **F)**.

3.6 Presence of the FTO obesity-risk alleles significantly influences browning gene expression profiles

Donor selection was based on the presence of obesity-risk SNP of the FTO locus, so donors 1 to 3, 4 to 6 and 7 to 9 carried a T/T risk-free, a T/C heterozygous or a C/C obesity-risk genotype, respectively. ProFAT analysis of the expression profile of white and browning marker genes revealed that 11 browning marker genes were significantly lower (*ACAA2*, *SLC25A20*, *ACO2*, *HADHB*, *ETFDH*, *SDHB*, *NDUFS1*, *ACADS*, *DLD*, *ETFB*, *PDHA1*) and two white markers (*ALCAM*, *HOXC8*) were significantly higher expressed in FTO C/C obesity-risk genotype **(Figure 6A**, red rectangle). Evaluation by BATLAS further highlighted FTO obesity-risk allele dependent differences, as 23 out of these genes were significantly lower expressed in samples carrying the FTO C/C obesity-risk allele **(Figure 6B**, red rectangle). Hierarchical cluster analyses based on Pearson correlation showed that 91% of the FTO T/T donor samples clustered together and 83% of the FTO C/C obesity-risk donor samples appeared in the same main cluster and they were closer to the preadipocytes, considering ProFAT genes **(Supplementary Figure S5A)**. BATLAS genes assembled very similarly, 75% of the FTO T/T and 83% of the FTO C/C donor samples clustered in the same main groups and FTO obesity-risk samples appeared closer to the non-thermogenic preadipocytes. Heterozygous samples appeared in either the FTO T/T or the C/C group **(Supplementary Figure 5B)**. The ProFAT and BATLAS data clearly suggest that hASCs which carry the FTO C/C obesity-risk genotype have significantly lower browning potential.

As a next step, we investigated all the DEGs based on the presence of the FTO obesity-risk allele in the white and brown differentiated DN and SC samples and 1295 DEGs were identified. The expression of 624 and 671 genes was significantly lower or higher, respectively, in the adipocytes which carried the risk alleles as compared to the non-risk allele carriers. The expression level of these genes was not as much influenced by the FTO status in the preadipocyte state suggesting that these genes have a functional role in the matured adipocytes **(Figure 6C)**. Analysis of these 1295 DEGs revealed that 81 code mitochondrial proteins, according to the Human MitoCarta 2.0 database [43] **(Supplementary Figure S5C)**. Out of those, 16 belong to one of the mitochondrial complexes and were lowly expressed in

bioRxiv preprint doi: https://doi.org/10.1101/2020.02.21.959593; this version posted April 9, 2020. The copyright holder for this preprint (which was not certified by peer review) is the author/funder, who has granted bioRxiv a license to display the preprint in perpetuity. It is made available under aCC-BY-NC-ND 4.0 International license.

the C/C obesity-risk genotype. Only six out of the 81 mitochondrial protein-encoding genes showed higher expression in the obesity-risk genotype (*SEPT4*, *PYCR1*, *PRELID2*, *CPT1A*, *MTHFD1L*, and *FKBP10*). Actually, the expression profile of genes encoding mitochondrial proteins (1035 genes in our samples, out of the 1158 genes in MitoCarta 2.0 database) visualized by heat map **(Supplementary Figure S5D)** also demonstrated that the majority of the mitochondrial genes were expressed at a lower extent in samples that carried the obesity-risk genotype. The genes *CKMT1A* and *CKMT1B*, which encode key mitochondrial creatine kinases and reported to be involved in UCP1-independent thermogenesis [4], were among those being significantly less expressed in FTO obesity-risk samples.

Among the genes that were expressed at lower levels in samples carrying the FTO obesity-risk allele, metabolic pathways were most affected including lipid metabolism, thermogenesis, carbon metabolism, oxidative phosphorylation, and degradation of certain amino acids such as valine, leucine and isoleucine **(Figures 6D** and **E)**. There was a striking resemblance between the set of network pathways negatively affected by the C/C genotype and those which were revealed by analyzing the ProFAT and BATLAS gene products **(Figures 6H-K)**. Furthermore, out of the 23 significantly enriched KEGG pathways defined by ProFAT genes, 21 were also found in BATLAS, and 19 of these are defined by genes that showed suppressed expression in FTO C/C samples. Out of the 29 KEGG pathways defined by BATLAS genes, 25 were also found in pathways determined by the lower expressed genes in C/C samples. Analyzing the Reactome pathways, similarly, high agreements could be found **(Supplementary Table S5A-B)**. Interactome network analysis of the lower expressed genes in FTO obesity-risk genotype suggests that under normal conditions, *DECR1* (dienoyl-CoA reductase), the chemokine *CCL2*, *LIPE*, *LDHB*, *SOD2*, *ATP5B* and *J* are central elements in maintaining connectivity **(Supplementary Table S6A)**. Genes that were linked to adipo- and thermogenesis such as *SLC2A4*, *EHHADH*, *PPARGC1A*, *CPT1B*, and *FABP4* appeared with high betweenness scores. In addition to the metabolic genes, a cytokine ligand, *CCL2*, and a receptor, *CXCR4*, also appeared as important critical components of this interactome network.

Comparing the FTO status-related gene expression patterns to upregulated DEGs in DN versus SC adipocytes, we found that out of the 529 genes (Groups 1 and 2) that were significantly higher in the DN samples, 33 genes were poorly expressed in the FTO obesity-risk genotype samples **(Figure 6L** and **Supplementary Table S7)**. Pathway analysis of genes with different expression based on tissue origin and presence of the FTO obesity-risk allele revealed that different pathways dominated the two. Interferon signaling and G-protein coupled rhodopsin-like receptors were the prominent DN specific pathways. The FTO C/C alleles influenced metabolic pathways, e.g. fatty acid and carbon metabolism. The 33 genes which had high expression in thermogenically more potent DN and appeared downregulated in the FTO obesity-risk genotype adipocytes underline the importance of PPAR signaling, lipid metabolism pathways (*CPT1B*, *FABP3*, *EHHADH*, *PLA2G4A*, *ZDHHC19*), creatine kinase activity (*CKMT1A* and *CKMT1B*), carboxylic acid metabolic processes (*HYAL1*) and sodium channel regulator activity (*SGK2*, *GPLD1*) in determining browning potential.

Since the presence of the FTO risk allele may lead to loss of restrain on the expression of genes related to thermogenesis and its regulation, we also looked for and found DEGs which showed higher expression in obesity-risk genotype samples **(Figures 6F** and **G)**. Clearly, the expression of genes related to the organization of the ECM was the most prominent upregulated pathway. This is consistent with the finding that ECM organization pathway has high importance in restraining the thermogenic potential (see gene expression and enrichment analyses in Groups 3 and 4 above and in preadipocytes). In addition, integrin cell surface

bioRxiv preprint doi: https://doi.org/10.1101/2020.02.21.959593; this version posted April 9, 2020. The copyright holder for this preprint (which was not certified by peer review) is the author/funder, who has granted bioRxiv a license to display the preprint in perpetuity. It is made available under aCC-BY-NC-ND 4.0 International license.

interaction, TGFB, PI3K-Akt and ras signaling also appeared among significantly enriched pathways in FTO obesity-risk samples. The network analysis clearly indicated the importance of fibronectin (*FN1* gene) for the integrity of this group of networks, but also the position and relationship of others such as *CTGF*, *BDNF*, *TGFB*, and *GLI1* **(Supplementary Table S6B)**; these growth and transcription factors regulate cell proliferation, differentiation and growth and can modulate the expression of other growth factors to determine cell fate. Considering the relationship between the DN downregulated genes and those expressed higher in C/C alleles, among the 520 genes (Groups 3 and 4) whose expression was lower in DN samples, 71 was higher in FTO obesity-risk samples **(Figure 6L** and **Supplementary Table S8)**. Again, the importance of ECM organization and, in particular, the collagen degradation and integrin cell surface interactions (*COL1A1*, *COL8A1*, *COL8A2*, *COL13A1*, *SDC1*, *ACAN*, *HAPLN1*, *ITGA11*) came into focus. By further analyses of these shared gene-sets, overexpressed pro-inflammatory cytokines and cytokine receptors (e.g. *IL11*, *IL20RA*, *IL27RA*) could be linked to less thermogenic DN adipocytes and thereby to obesity and inflammation [44]. Finally, *IRX3*, which was already described as a negative [19] and positive [45] regulator of the development of thermogenic adipocytes, was also among the genes kept lowly expressed in DN and FTO T/T adipocytes but became higher expressed in the adipocytes with the obesity-risk genotype.

bioRxiv preprint doi: https://doi.org/10.1101/2020.02.21.959593; this version posted April 9, 2020. The copyright holder for this preprint (which was not certified by peer review) is the author/funder, who has granted bioRxiv a license to display the preprint in perpetuity. It is made available under aCC-BY-NC-ND 4.0 International license.

4. DISCUSSION

Human ASCs from distinct fat depots have the potential to undergo a browning program [14]. One of the major sites that contain active BAT in humans is located in the neck, particularly in its deep regions [14,46]. When we compared SC and DN adipocyte progenitors from human neck, the latter had greater browning potential, in accordance with previous findings [18,36,47,48]. On the other hand, SC hASCs were also able to build up a significant thermogenic competency. The difference between SC and DN hASCs in the capability of building a thermogenic potential might be explained by their differential depot-specific epigenetic chromatin signatures. Divoux et al. reported that subcutaneous preadipocytes cultivated from abdominal and gluteofemoral fat of six overweight or obese women had depot-specific chromatin structures resulting in gene expression patterns that were selective for the anatomical identity of the cells [49]. Primarily, we found 1420 DEGs when the hASCs of SC and DN origins were compared. This relatively large number of DEGs and their designated pathways suggest that the two anatomically localized tissues have cells of different epigenetic signatures even at precursor level and presumably have a specific ECM structure that is maintained *ex vivo* after differentiation. The organization of the ECM is differently regulated: degradation processes are prominent in the SC samples, whereas in DN samples ECM reorganization and regulation of vascular development appear to be significant. The retinoic acid signaling pathway also appeared in DN cells both at progenitor and at differentiated states; its role in inducing thermogenesis via increasing angiogenesis by activating VEGFA/VEGFR2 signaling has been suggested but not explored in details [50,51].

Many genes were already proposed to predispose cells to a higher or lower thermogenic potential at the precursor level [48,52-54]. Similarly to these results in our samples, *EBF2*, *LHX8*, *MEOX2*, *TBX15* showed higher expression in DN preadipocytes, while *HOXC8*, *HOXC9*, *DTP*, and *IGFBP3* were pronounced in SC ones. Several white and brown predisposing marker genes identified by Xue et al. [48] were also differentially expressed in our SC and DN preadipocytes, such as *S1PR3*, *GPRC5A*, *MASP1*, *C10orf90*, *ST6GALNAC3*, and *SVIL* having higher expression in DN, whereas *COL12A1*, *SHROOM3*, *GRIK2*, and *HAPLN1* were being enriched in SC precursors. However, the 26 white and 25 brown predisposing marker genes pointed out by this group are highly diverse in their function and no determining pathways can be identified from the gene set that would underpin future thermogenic activity [48].

Recently, two global approaches based on mouse and human experimental data have identified sets of genes (50 in ProFAT and 119 in BATLAS), the expression pattern of which could be used, also by us, to determine the browning potential of adipocyte cells or tissues [21,22]. Surprisingly, the number of common genes in the two lists is very small, only 17. However, we found that ProFAT and BATLAS gene products are actually part of very similar pathways linked to increased metabolic activity as defined by KEGG or REACTOM, suggesting that it may be more appropriate to focus on gene-defined pathways, biological processes or specific cell components for better defining adipocyte browning.

In this study, we considered three different influences (anatomical origin, PPARγ stimulation by rosiglitazone and alleles of the rs1421085 FTO locus) asking what pathways and processes they induce for increased browning. Regarding site-specific gene expression, we can conclude that among the 1049 DEGs in DN versus SC samples, several classical brown and beige markers are greatly co-expressed in mature DN adipocytes, e.g. *PRDM16*, *LHX8*, *EBF2*, *TBX1*, *KCNK3*, *CITED1*, and *MTUS1*. The brown markers *LHX8* [16], *PRDM16* [12,55] and

bioRxiv preprint doi: https://doi.org/10.1101/2020.02.21.959593; this version posted April 9, 2020. The copyright holder for this preprint (which was not certified by peer review) is the author/funder, who has granted bioRxiv a license to display the preprint in perpetuity. It is made available under aCC-BY-NC-ND 4.0 International license.

EBF2 [52,53] also showed significantly higher expression in the DN samples, while the beige marker *TBX1* [17] had a similar pattern. Interestingly, several well-known thermogenic markers, including *ELOVL3* [56] and *PPARGC1A* [57] were not expressed differently in SC and DN adipocytes. A few brown marker genes had higher expression in SC samples differentiated by white protocol (*DIO2* [1], *HSPB7*, *EVA1A* [58]) and *ZIC1* [16] was barely expressed in all samples. Our findings are in line with the conclusions of Jespersen et al. [18] who claimed there is an overlap signature between classical murine brown and beige marker genes in adipocytes in the DN region of adult humans.

Among the pathways identified by 1049 DEGs comparing SC and DN samples, the differential regulation of ECM organization is a characteristic feature of adipocytes of the two origins, suggesting site-specific organization of the ECM, which is maintained even when the cells are differentiated *ex vivo*. This points out that conditions used in the cell culture, such as the quality of plates, application of biomaterials or scaffold-based 3D culture technics may significantly influence the ECM organization and consequently cellular functions and suggests that efforts should be made to use culture methods that are the most consistent with *in vivo* conditions. In addition, signaling transmitted by class A1 rhodopsin-like receptors and interferon alpha/beta receptors, which were expressed higher in DN samples, and neuroactive ligand receptors, ras proximate 1 (RAP1) G-protein and cGMP molecules which appeared elevated in SC samples, may be critical in establishing of the different functional properties of DN and SC adipocytes. The significantly enriched interferon, cytokine and other signaling pathways in DN adipocytes suggest that the anatomical origin of the progenitors determine extrinsic factors involved in cell-cell communication rather than the metabolic properties of the browning adipocytes. There are several secreted factors which were already reported to positively influence browning in an autocrine manner [59].

Alternative sources of mesenchymal stem cells (MSCs), e.g. the oral derived MSCs are able to release immunomodulatory and trophic molecules which support regeneration of damaged tissues [60]. In the future, these less invasively harvestable MSCs, which have great potential in regenerative medicine, might be used to conduct studies with regard to adipocyte browning [61]. However, our data indicate that the tissue origin of the progenitors may significantly affect the results of the studies, which could give uncertainty in experiments using induced pluripotent stem cells (iPSC) or other non-adipose-derived MSCs [61,62]. It also suggests that it is preferable to use cells obtained from tissues with high thermogenic potential in future brown adipocyte transplantation and regenerative assays. MSCs isolated from various tissues have distinct differentiation potential and usually pathways that reflect the original tissue are preferred.

We found 217 genes that were upregulated either in SC or DN adipocytes in response to the brown protocol with sustained rosiglitazone treatment. Eighty of these genes (and the PPAR signaling pathway) were significantly upregulated in adipocytes of both origins, including *KLF11*, *TSHR*, *PDK4*, *APOL6*, *CPT1B*, and *CIDEA* that showed elevated expression in response to rosiglitazone in browning hMADS-derived adipocytes as well as a result of the formation of PPARγ super-enhancers [40]. Our data suggest that KLF11-dependent super-enhancers are assembled upon rosiglitazone treatment in both types of primary adipocytes from the neck.

Another super-enhancer, which is located on an obesity-risk associated locus of the intronic region of the FTO gene, was linked to the regulation of browning in subcutaneous fat [19,45,63,64] by determining the level of IRX3 and IRX5. The role of IRX3 and 5 in this

bioRxiv preprint doi: https://doi.org/10.1101/2020.02.21.959593; this version posted April 9, 2020. The copyright holder for this preprint (which was not certified by peer review) is the author/funder, who has granted bioRxiv a license to display the preprint in perpetuity. It is made available under aCC-BY-NC-ND 4.0 International license.

signaling pathway is still controversial [19,45,63]. In our study, *IRX3* was significantly higher expressed in samples with FTO obesity-risk alleles and support its suppressive role in thermogenesis. Overall, the expression profile and pathway analysis of the 1295 DEGs related to the absence and presence of the C/C alleles, clearly points to major difference in regulation of metabolism including mitochondrial biological processes. Out of these, 624 genes (e.g. *CKMT1A/B*, *CITED1*, *PPARGC1A/B*, and *CPT1B*) were lower expressed in those adipocytes that carried the obesity-risk genotype and the enriched pathways (maintained by the normal T/T genotype) included fatty acid metabolism, thermogenesis, respiratory electron transport and the signaling by retinoic acid (which showed DN specific appearance as well). Surprisingly, the enriched pathways identified by these gene expression patterns include almost entirely the pathways defined by the BATLAS and ProFAT brown marker genes **(Supplementary Table S5A-B)** which suggest that this genetic predisposition has a pivotal importance in determining thermogenic competency of adipocytes from the neck. In addition to the regulation of metabolic pathways, the organization of the ECM and various signaling pathways (RAP1, Ras, Hippo, Relaxin, TGF-beta, PI3-Akt) appears to be greatly affected by the risk alleles. In spite of the existing 104 similarly expressed DEGs in the comparisons of FTO T/T vs C/C genotypes and DN vs SC adipocytes **(Supplementary Figure S6)**, FTO genotypes define largely different gene expression patterns and pathways compared to those recognized on the basis of tissue origin.

Comparing the results of the three different analytic approach used for characterization of gene expression patterns linked to browning (by anatomical origin, PPARγ stimulation and presence of the rs1421085 FTO locus), only five transcripts (carnitine palmitoyltransferase 1B, creatine kinase mitochondrial 1B, thiamine transporter 2, family with sequence similarity 189 Member A2, and long intergenic non-protein coding RNA 2458) were expressed higher in brown adipocytes determined by all of the three conditions **(Supplementary Figure S6)**. Only one gene, Collagen alpha-1(VIII) chain was significantly higher expressed in those samples that showed lower thermogenic activity. The low number of common genes and pathways suggests that these three factors elicit significantly different responses in cells in contribution to the browning transcriptome and phenotype. Interestingly, the tissue origin resulted in about two times (2.2x) more DEGs, presumably associated with browning, than PPARγ stimulation. It is striking that the absence or presence of the FTO obesity-risk allele results in the greatest difference in the gene expression profile (1295 genes) of the differentiated cells **(Supplementary Figure S6)**. Consequently, research efforts targeting the regulatory system determined by the rs1421085 FTO locus have the potential to develop novel therapeutic approaches for increasing weight loss by thermogenesis in obese patients.

UCP1-independent energy releasing processes were recently described in adipocytes, which may provide an alternative way to reduce obesity. Our RNA sequencing data showed that *CKMT1A* and *B*, futile cycle maintaining creatine kinases [4], were expressed higher in DN as compared to SC adipocytes and less abundant in those that had an obesity-risk genotype of the rs1421085 FTO locus. *PM20D1* encodes an enzyme that catalyzes the synthesis of N-lipidated/N-fatty-acyl amino acids which function as endogenous uncouplers of mitochondrial respiration in a UCP1-independent manner [6]; it was expressed higher in DN brown adipocytes and rosiglitazone increased its expression in both SC and DN adipocytes regardless of the FTO allele status. This specific effect of the PPARγ-agonist was observed in other studies as well [9,41].

We found several genes with enriched expression in DN as compared to SC adipocytes which have not been directly linked to browning so far. The product of relaxin receptor 2 (RXFP2)

bioRxiv preprint doi: https://doi.org/10.1101/2020.02.21.959593; this version posted April 9, 2020. The copyright holder for this preprint (which was not certified by peer review) is the author/funder, who has granted bioRxiv a license to display the preprint in perpetuity. It is made available under aCC-BY-NC-ND 4.0 International license.

mediates G-protein dependent stimulation of adenylate cyclase and an increase of cAMP levels [65]. Receptor-type tyrosine-protein phosphatase N2 (PTPRN2) was shown to act as an autoantigen in type I diabetes and required for the accumulation of insulin-containing vesicles preventing their degradation in rat gastrointestinal endocrine cells [66] and also has a role in the accumulation of norepinephrine, dopamine and serotonin in autonomic nerve endings [67]. Ephrin type-A receptor 5 (EPHA5) which has a role in regulation of insulin secretion [68] was also highly expressed in DN as compared to SC brown adipocytes. Cysteinyl leukotriene receptor 2 (CYSLTR2) was shown to induce type 2 immune response in an interleukin (IL)-33 dependent manner [69]; this response was proposed but also debated to be a positive regulator of browning in mice [70,71]. In our experiments, transcripts of both genes were enriched in DN adipocytes. Further investigations are needed to confirm the direct role of these genes in the browning process.

bioRxiv preprint doi: https://doi.org/10.1101/2020.02.21.959593; this version posted April 9, 2020. The copyright holder for this preprint (which was not certified by peer review) is the author/funder, who has granted bioRxiv a license to display the preprint in perpetuity. It is made available under aCC-BY-NC-ND 4.0 International license.

5. ACKNOWLEDGEMENTS

We thank Dr. Tibor Nagy and Dr. Zoltán Barta for his help and advice in analyzing the data, Dr. Endre Barta for reviewing the manuscript and Jennifer Nagy for technical assistance.

Funding: This work was supported by the European Union and the European Regional Development Fund [GINOP-2.3.2-15-2016-00006], Ministry for Innovation and Technology in Hungary [FIKP_20428-3_2018_FELITSTRAT and EFOP-3.6.3-VEKOP-16-2017-00009] and the Hungarian Research Fund [OTKA-FK131424 and K129139]. E.K. was supported by the János Bolyai Fellowship of the Hungarian Academy of Sciences and the ÚNKP-19-4 New National Excellence Program of the Ministry for Innovation and Technology in Hungary. All of the funders had not any role in study design, data collection, data analysis, interpretation, and writing of the report.

6. CONFLICTS OF INTEREST

The authors declare no competing interests with relevance to this study.

bioRxiv preprint doi: https://doi.org/10.1101/2020.02.21.959593; this version posted April 9, 2020. The copyright holder for this preprint (which was not certified by peer review) is the author/funder, who has granted bioRxiv a license to display the preprint in perpetuity. It is made available under aCC-BY-NC-ND 4.0 International license.

7. REFERENCES

[1] Cannon, B., Nedergaard, J., 2004. Brown adipose tissue: function and physiological significance. Physiological Reviews 84:277–359.
[2] Kajimura, S., Spiegelman, B.M., Seale, P., 2015. Brown and Beige Fat: Physiological Roles beyond Heat Generation. Cell Metabolism 22:546–559.
[3] Fedorenko, A., Lishko, P.V., Kirichok, Y., 2012. Mechanism of fatty-acid-dependent UCP1 uncoupling in brown fat mitochondria. Cell 151:400–413.
[4] Kazak, L., Chouchani, E.T., Jedrychowski, M.P., Erickson, B.K., Shinoda, K., Cohen, P., Vetrivelan, R., Lu, G.Z., Laznik-Bogoslavski, D., Hasenfuss, S.C., Kajimura, S., Gygi S.P., Spiegelman, B.M., 2015. A creatine-driven substrate cycle enhances energy expenditure and thermogenesis in beige fat. Cell 163:643–655.
[5] Kazak, L., Chouchani, E.T., Lu, G.Z., Jedrychowski, M.P., Bare, C.J., Mina, A.I., Kumari, M., Zhang, S., Vuckovic, I., Laznik-Bogoslavski, D., Dzeja, P., Banks, A.S., Rosen, E.D., Spiegelman, B.M., 2017. Genetic Depletion of Adipocyte Creatine Metabolism Inhibits Diet-Induced Thermogenesis and Drives Obesity. Cell Metabolism 26:660–671.e3.
[6] Kristóf, E., Doan-Xuan, Q.M., Sárvári, A.K., Klusóczki, Á., Fischer-Posovszky, P., Wabitsch, M., Bacso, Z., Bai, P., Balajthy, Z., Fésüs, L., 2016. Clozapine modifies the differentiation program of human adipocytes inducing browning. Translational Psychiatry 6:e963.
[7] Klusóczki, Á., Veréb, Z., Vámos, A., Fischer-Posovszky, P., Wabitsch, M., Bacso, Z., Fésüs, L., Kristóf, E., 2019. Differentiating SGBS adipocytes respond to PPARγ stimulation, irisin and BMP7 by functional browning and beige characteristics. Scientific Reports 9:5823.
[8] Ikeda, K., Kang, Q., Yoneshiro, T., Camporez, J.P., Maki, H., Homma, M., Shinoda, K., Chen, Y., Lu, X., Maretich, P., Tajima, K., Ajuwon, K.M., Soga, T., Kajimura, S., 2017. UCP1-independent signaling involving SERCA2b-mediated calcium cycling regulates beige fat thermogenesis and systemic glucose homeostasis. Nature Medicine 23:1454–1465.
[9] Long, J.Z., Svensson, K.J., Bateman, L.A., Lin, H., Kamenecka, T. Lokurkar, I.A., Lou, J., Rao, R.R., Chang, M.R., Jedrychowski, M.P., Paulo, J.A., Gygi S.P., Griffin, P.R., Nomura, D.K., Spiegelman, B.M., 2016. The Secreted Enzyme PM20D1 Regulates Lipidated Amino Acid Uncouplers of Mitochondria. Cell 166:424–435.
[10] Harms, M., Seale, P., 2013. Brown and beige fat: development, function and therapeutic potential. Nature Medicine 19:1252–1263.
[11] Whittle, A.J., López, M., Vidal-Puig, A., 2011. Using brown adipose tissue to treat obesity - the central issue. Trends in Molecular Medicine 17: 405–411.
[12] Seale, P., Bjork, B., Yang, W., Kajimura, S., Chin, S., Kuang, S., Scimè, A., Devarakonda, S., Conroe, H.M., Erdjument-Bromage, H., Tempst, P., Rudnicki, M.A., Beier, D.R., Spiegelman, B.M., 2008. PRDM16 controls a brown fat/skeletal muscle switch. Nature 454:961–967.
[13] Petrovic, N., Walden, T.B., Shabalina, I.G., Timmons, J.A., Cannon, B., Nedergaard, J., 2010. Chronic peroxisome proliferator-activated receptor gamma (PPARgamma) activation of epididymally derived white adipocyte cultures reveals a population of thermogenically competent, UCP1-containing adipocytes molecularly distinct from classic brown adipocytes. Journal of Biological Chemistry 285:7153–7164.
[14] Leitner, B.P., Huang, S., Brychta, R.J., Duckworth, C.J, Baskin, A.S., McGehee, S., Tal, I., Dieckmann, W., Gupta, G., Kolodny, G.M., Pacak, K., Herscovitch, P., Cypess, A.M., Chen K.Y., 2017. Mapping of human brown adipose tissue in lean and obese young men. PNAS 114:8649–8654.

bioRxiv preprint doi: https://doi.org/10.1101/2020.02.21.959593; this version posted April 9, 2020. The copyright holder for this preprint (which was not certified by peer review) is the author/funder, who has granted bioRxiv a license to display the preprint in perpetuity. It is made available under aCC-BY-NC-ND 4.0 International license.

[15] Svensson, P.A., Jernås, M., Sjöholm, K., Hoffmann, J.M., Nilsson, B.E., Hansson, M., Carlsson, L.M.S., 2011. Gene expression in human brown adipose tissue. International Journal of Molecular Medicine 27:227–232.
[16] Cypess, A.M., White, A.P., Vernochet, C., Schulz, T.J., Xue, R., Sass, C.A., Huang, T.L., Roberts-Toler, C., Weiner, L.S., Sze, C., Chacko, A.T., Deschamps, L.N., Herder, L.M., Truchan, N., Glasgow, A.L., Holman, A.R., Gavrila, A., Hasselgren, P.O., Mori, M.A., Molla, M., Tseng, Y.H., 2013. Anatomical localization, gene expression profiling and functional characterization of adult human neck brown fat. Nature Medicine 19:635–639.
[17] Wu, J., Boström, P., Sparks, L.M., Ye, L., Choi, J.H., Giang, A.H., Khandekar, M., Virtanen, K.A., Nuutila, P., Schaart, G., Huang, K., Tu, H., van Marken Lichtenbelt, W.D., Hoeks, J., Enerbäck, S., Schrauwen, P., Spiegelman, B.M., 2012. Beige adipocytes are a distinct type of thermogenic fat cell in mouse and human. Cell 150:366–376.
[18] Jespersen, N.Z., Larsen, T.J., Peijs, L., Daugaard, S., Homøe, P., Loft, A., de Jong, J., Mathur, N., Cannon, B., Nedergaard, J., Pedersen, B.K., Møller, K., Scheele, C., 2013. A classical brown adipose tissue mRNA signature partly overlaps with brite in the supraclavicular region of adult humans. Cell Metabolism 17:798–805.
[19] Claussnitzer, M., Dankel, S.N., Kim, K.H., Quon, G., Meuleman, W., Haugen, C., Glunk, V., Sousa, I.S., Beaudry, J.L., Puviindran, V., Abdennur, N.A., Liu, J., Svensson, P.A., Hsu, Y.H., Drucker, D.J., Mellgren, G., Hui, C.C., Hauner, H., Kellis, M., 2015. FTO Obesity Variant Circuitry and Adipocyte Browning in Humans. The New England Journal of Medicine 373:895–907.
[20] Min, S.Y., Desai, A., Yang, Z., Sharma, A., DeSouza, T., Genga, R.M.J., Kucukural, A., Lifshitz, L.M., Nielsen, S., Scheele, C., Maehr, R., Garber, M., Corvera, S., 2019. Diverse repertoire of human adipocyte subtypes develops from transcriptionally distinct mesenchymal progenitor cells. PNAS 116:17970–17979.
[21] Perdikari, A., Leparc, G.G., Balaz, M., Pires, N.D., Lidell, M.E., Sun, W., Fernandez-Albert, F., Müller, S., Akchiche, N., Dong, H., Balazova, L., Opitz, L., Röder, E., Klein, H., Stefanicka, P., Varga, L., Nuutila, P., Virtanen, K.A., Niemi, T., Taittonen, M., Rudofsky, G., Ukropec, J., Enerbäck, S., Stupka, E., Neubauer, H., Wolfrum, C., 2018. BATLAS: Deconvoluting Brown Adipose Tissue. Cell Reports 25:784–797.e4.
[22] Cheng, Y., Jiang, L., Keipert, S., Zhang, S., Hauser, A., Graf, E., Strom, T., Tschöp, M., Jastroch, M., Perocchi, F., 2018. Prediction of Adipose Browning Capacity by Systematic Integration of Transcriptional Profiles. Cell Reports 23:3112–3125.
[23] Rask-Andersen, M., Karlsson, T., Ek, W.E., Johansson, Å., 2019. Genome-wide association study of body fat distribution identifies adiposity loci and sex-specific genetic effects. Nature Communications 10:339.
[24] Hallberg, M., Morganstein, D.L., Kiskinis, E., Shah, K., Kralli, A., Dilworth, S.M., White, R., Parker, M.G., Christian, M., 2008. A functional interaction between RIP140 and PGC-1alpha regulates the expression of the lipid droplet protein CIDEA. Molecular and Cellular Biology 28:6785–6795.
[25] Sharp, L.Z., Shinoda, K., Ohno, H., Scheel, D.W., Tomoda, E., Ruiz, L., Hu, H., Wang, L., Pavlova, Z., Gilsanz, V., Kajimura, S., 2012. Human BAT possesses molecular signatures that resemble beige/brite cells. PLoS One 7:e49452.
[26] Kristóf, E., Klusóczki, Á., Veress, R., Shaw, A., Combi, Z.S., Varga, K., Győry, F., Balajthy, Z., Bai, P., Bacso, Z., Fésüs, L., 2019. Interleukin-6 released from differentiating human beige adipocytes improves browning. Experimental Cell Research 377:47–55.
[27] Kristóf, E., Doan-Xuan, Q.M., Bai, P., Bacso, Z., Fésüs, L., 2015. Laser-scanning cytometry can quantify human adipocyte browning and proves effectiveness of irisin. Scientific Reports 5:12540.

bioRxiv preprint doi: https://doi.org/10.1101/2020.02.21.959593; this version posted April 9, 2020. The copyright holder for this preprint (which was not certified by peer review) is the author/funder, who has granted bioRxiv a license to display the preprint in perpetuity. It is made available under aCC-BY-NC-ND 4.0 International license.

[28] Fischer-Posovszky, P., Newell, F.S., Wabitsch, M., Tornqvist, H.E., 2008. Human SGBS cells - a unique tool for studies of human fat cell biology. Obesity Facts 1:184–189.
[29] Elabd, C., Chiellini, C., Carmona, M., Galitzky, J., Cochet, O., Petersen, R., Pénicaud, L., Kristiansen, K., Bouloumié, A., Casteilla, L., Dani, C., Ailhaud, G., Amri, E.Z., 2009. Human multipotent adipose-derived stem cells differentiate into functional brown adipocytes. Stem Cells 27:2753–2760.
[30] Sárvári, A.K., Veréb, Z., Uray, I.P., Fésüs, L., Balajthy, Z., 2014. Atypical antipsychotics induce both proinflammatory and adipogenic gene expression in human adipocytes in vitro. Biochemical and Biophysical Research Communications 450:1383–1389.
[31] Dobin, A., Davis, C.A., Schlesinger, F., Drenkow, J., Zaleski, C., Jha, S., Batut, P., Chaisson, M., Gingeras, T.R., 2013. STAR: ultrafast universal RNA-seq aligner. Bioinformatics 29:15–21.
[32] Liao, Y., Smyth, G.K., Shi, W., 2014. featureCounts: an efficient general purpose program for assigning sequence reads to genomic features. Bioinformatics 30:923–930.
[33] Love, M.I., Huber, W., Anders, S., 2014. Moderated estimation of fold change and dispersion for RNA-seq data with DESeq2. Genome Biology 15:550.
[34] Doan-Xuan, Q.M., Sarvari, A.K., Fischer-Posovszky, P., Wabitsch, M., Balajthy, Z., Fésüs, L., Bacso, Z., 2013. High content analysis of differentiation and cell death in human adipocytes. Cytometry A 83: 933–943.
[35] Anders, S., Huber, W., 2010. Differential expression analysis for sequence count data. Genome Biology 11:R106.
[36] Tews, D., Schwar, V., Scheithauer, M., Weber, T., Fromme, T., Klingenspor, M., Barth, T.F., Möller, P., Holzmann, K., Debatin, K.M., Fischer-Posovszky, P., Wabitsch, M., 2014. Comparative gene array analysis of progenitor cells from human paired deep neck and subcutaneous adipose tissue. Molecular and Cellular Endocrinology 395:41–50.
[37] Lowe, C.E., O'Rahilly, S., Rochford, J.J., 2011. Adipogenesis at a glance. Journal of Cell Science 124:2681–2686.
[38] Blázquez-Medela, A.M., Jumabay, M., Boström, K.I., 2019. Beyond the bone: Bone morphogenetic protein signaling in adipose tissue. Obesity Reviews 20:648–658.
[39] Wang, H., Sreenivasan, U., Hu, H., Saladino, A., Polster, B.M., Lund, L.M., Gong, D.W., Stanley, W.C., Sztalryd, C., 2011. Perilipin 5, a lipid droplet-associated protein, provides physical and metabolic linkage to mitochondria. Journal of Lipid Research 52:2159–2168.
[40] Loft, A., Forss, I., Siersbæk, M.S., Schmidt, S.F., Larsen, A.S.B., Madsen, J.G.S., Pisani, D.F., Nielsen, R., Aagaard, M.M., Mathison, A., Neville, M.J., Urrutia, R., Karpe, F., Amri, E.Z., Mandrup, S., 2015. Browning of human adipocytes requires KLF11 and reprogramming of PPARγ superenhancers. Genes & Development 29:7–22.
[41] Benson, K.K., Hu, W., Weller, A.H., Bennett, A.H., Chen, E.R., Khetarpal, S.A., Yoshino, S., Bone, W.P., Wang, L., Rabinowitz, J.D., Voight, B.F., Soccio, R.E., 2019. Natural human genetic variation determines basal and inducible expression of PM20D1, an obesity-associated gene. PNAS 116:23232–23242.
[42] Simcox, J., Geoghegan, G., Maschek, J.A., Bensard, C.L., Pasquali, M., Miao, R., Lee, S., Jiang, L., Huck, I., Kershaw, E.E., Donato, A.J., Apte, U., Longo, N., Rutter, J., Schreiber, R., Zechner, R., Cox, J., Villanueva, C.J., 2017. Global Analysis of Plasma Lipids Identifies Liver-Derived Acylcarnitines as a Fuel Source for Brown Fat Thermogenesis. Cell Metabolism 26:509–522.e6.
[43] Calvo, S.E., Clauser, K.R., Mootha, V.K., 2016. MitoCarta2.0: an updated inventory of mammalian mitochondrial proteins. Nucleic Acids Research 44:D1251–1257.
[44] Hotamisligil, G.S., 2006. Inflammation and metabolic disorders. Nature 444:860–867.

bioRxiv preprint doi: https://doi.org/10.1101/2020.02.21.959593; this version posted April 9, 2020. The copyright holder for this preprint (which was not certified by peer review) is the author/funder, who has granted bioRxiv a license to display the preprint in perpetuity. It is made available under aCC-BY-NC-ND 4.0 International license.

[45] Zou, Y., Lu, P., Shi, J., Liu, W., Yang, M., Zhao, S., Chen, N., Chen, M., Sun, Y., Gao, A., Chen, Q., Zhang, Z., Ma, Q., Ning, T., Ying, X., Jin, J., Deng, X., Shen, B., Zhang, Y., Yuan, B., Kauderer, S., Liu, S., Hong, J., Liu, R., Ning, G., Wang, W., Gu, W., Wang, J., 2017. IRX3 Promotes the Browning of White Adipocytes and Its Rare Variants are Associated with Human Obesity Risk. EBioMedicine 24:64–75.
[46] Cypess, A.M., Lehman, S., Williams, G., Tal I., Rodman, D., Goldfine, A.B., Kuo, F.C., Palmer, E.L., Tseng, Y.H., Doria, A., Kolodny, G.M., Kahn, C.R., 2009. Identification and importance of brown adipose tissue in adult humans. The New England Journal of Medicine 360:1509–1517.
[47] Shinoda, K., Luijten, I.H., Hasegawa, Y., Hong, H., Sonne, S.B., Kim, M., Xue, R., Chondronikola, M., Cypess, A.M., Tseng, Y.H., Nedergaard, J., Sidossis, L.S., Kajimura, S., 2015. Genetic and functional characterization of clonally derived adult human brown adipocytes. Nature Medicine 21:389–394.
[48] Xue, R., Lynes, M.D., Dreyfuss, J.M., Shamsi, F., Schulz, T.J., Zhang, H., Huang, T.L., Townsend, K.L., Li, Y., Takahashi, H., Weiner, L.S., White, A.P., Lynes, M.S., Rubin, L.L., Goodyear, L.J., Cypess, A.M., Tseng, Y.H., 2015. Clonal analyses and gene profiling identify genetic biomarkers of the thermogenic potential of human brown and white preadipocytes. Nature Medicine 21:760–768.
[49] Divoux, A., Sandor, K., Bojcsuk, D., Talukder, A., Li, X., Balint, B.L., Osborne, T.F., Smith, S.R., 2018. Differential open chromatin profile and transcriptomic signature define depot-specific human subcutaneous preadipocytes: primary outcomes. Clinical Epigenetics 10, 148.
[50] Wang, B., Fu, X., Liang, X., Deavila, J.M., Wang, Z., Zhao, L., Tian, Q., Zhao, J., Gomez, N.A., Trombetta, S.C., Zhu, M.J., Du, M., 2017. Retinoic acid induces white adipose tissue browning by increasing adipose vascularity and inducing beige adipogenesis of PDGFRα+ adipose progenitors. Cell Discovery 3:17036.
[51] Mercader, J., Ribot, J., Murano, I., Felipe, F., Cinti, S., Bonet, M.L., Palou A., 2006. Remodeling of white adipose tissue after retinoic acid administration in mice. Endocrinology 147:5325–5332.
[52] Wang, W., Kissig, M., Rajakumari, S., Huang, L., Lim, H.W., Won, K.J., Seale, P., 2014. Ebf2 is a selective marker of brown and beige adipogenic precursor cells. PNAS 111:14466–14471.
[53] Stine, R.R., Shapira, S.N., Lim, H.W., Ishibashi, J., Harms, M., Won, K.J., Seale, P., 2015. EBF2 promotes the recruitment of beige adipocytes in white adipose tissue. Molecular Metabolism 5:57–65.
[54] Timmons, J.A., Wennmalm, K., Larsson, O., Walden, T.B., Lassmann, T., Petrovic, N., Hamilton, D.L., Gimeno, R.E., Wahlestedt, C., Baar, K., Nedergaard, J., Cannon, B., 2007. Myogenic gene expression signature establishes that brown and white adipocytes originate from distinct cell lineages. PNAS 104:4401–4406.
[55] Seale, P., Kajimura, S., Yang, W., Chin, S., Rohas, L.M., Uldry, M., Tavernier, G., Langin, D., Spiegelman, B.M., 2007. Transcriptional control of brown fat determination by PRDM16. Cell Metabolism 6:38–54.
[56] Tvrdik, P., Asadi, A., Kozak, L.P., Nedergaard, J., Cannon, B., Jacobsson, A., 1997. Cig30, a mouse member of a novel membrane protein gene family, is involved in the recruitment of brown adipose tissue. Journal of Biological Chemistry 272:31738–31746.
[57] Puigserver, P., Wu, Z., Park, C.W., Graves, R., Wright, M., Spiegelman, B.M., 1998. A cold-inducible coactivator of nuclear receptors linked to adaptive thermogenesis. Cell 92:829–839.
[58] Park, A., Kim, W.K., Bae, K.H., 2014. Distinction of white, beige and brown adipocytes derived from mesenchymal stem cells. World Journal of Stem Cells 6:33–42.

bioRxiv preprint doi: https://doi.org/10.1101/2020.02.21.959593; this version posted April 9, 2020. The copyright holder for this preprint (which was not certified by peer review) is the author/funder, who has granted bioRxiv a license to display the preprint in perpetuity. It is made available under aCC-BY-NC-ND 4.0 International license.

[59] Villarroya, J., Cereijo, R., Gavaldà-Navarro, A., Peyrou, M., Giralt, M., Villarroya, F., 2019. New insights into the secretory functions of brown adipose tissue. Journal of Endocrinology pii:JOE–19–0295.R1.
[60] Figueroa, F.E., Carrión, F., Villanueva, S., Khoury, M., 2012. Mesenchymal stem cell treatment for autoimmune diseases: a critical review. Biological Research 45:269–277.
[61] Tatullo, M., Codispoti, B., Pacifici, A., Palmieri, F., Marrelli, M., Pacifici, L., Paduano, F., 2017. Potential Use of Human Periapical Cyst-Mesenchymal Stem Cells (hPCy-MSCs) as a Novel Stem Cell Source for Regenerative Medicine Applications. Frontiers in Cell and Developmental Biology 5:103.
[62] Mohsen-Kanson, T., Hafner, A.L., Wdziekonski, B., Takashima, Y., Villageois, P., Carrière, A., Svensson, M., Bagnis, C., Chignon-Sicard, B., Svensson, P.A., Casteilla, L., Smith, A., Dani, C., 2014. Differentiation of human induced pluripotent stem cells into brown and white adipocytes: role of Pax3. Stem Cells 32:1459–1467.
[63] Bjune, J.I., Haugen, C., Gudbrandsen, O., Nordbø, O.P., Nielsen, H.J., Våge, V., Njølstad, P.R., Sagen, J.V., Dankel, S.N., Mellgren, G., 2019. IRX5 regulates adipocyte amyloid precursor protein and mitochondrial respiration in obesity. International Journal of Obesity (London) 43:2151–2162.
[64] Smemo, S., Tena, J.J., Kim, K.H., Gamazon, E.R., Sakabe, N.J., Gómez-Marín, C., Aneas, I., Credidio, F.L., Sobreira, D.R., Wasserman, N.F., Lee, J.H., Puviindran, V., Tam, D., Shen, M., Son, J.E., Vakili N.A., Sung, H.K., Naranjo, S., Acemel, R.D., Manzanares, M., Nagy, A., Cox, N.J., Hui, C.C., Gomez-Skarmeta, J.L., Nóbrega, M.A., 2014. Obesity-associated variants within FTO form long-range functional connections with IRX3. Nature 507:371–375.
[65] Hartley, B.J., Scott, D.J., Callander, G.E., Wilkinson, T.N., Ganella, D.E., Kong, C.K., Layfield, S., Ferraro, T., Petrie, E.J., Bathgate, R.A.D., 2009. Resolving the unconventional mechanisms underlying RXFP1 and RXFP2 receptor function. Annals of the New York Academy of Sciences 1160:67–73.
[66] Torii, S., Kubota, C., Saito, N., Kawano, A., Hou, N., Kobayashi, M., Torii, R., Hosaka, M., Kitamura, T., Takeuchi, T., Gomi, H., 2018. The pseudophosphatase phogrin enables glucose-stimulated insulin signaling in pancreatic β cells. Journal of Biological Chemistry 293:5920–5933.
[67] Gomi, H., Kubota-Murata, C., Yasui, T., Tsukise, A., Torii, S., 2013. Immunohistochemical analysis of IA-2 family of protein tyrosine phosphatases in rat gastrointestinal endocrine cells. Journal of Histochemistry and Cytochemistry 61:156–168.
[68] Jain, R., Jain, D., Liu, Q., Bartosinska, B., Wang, J., Schumann, D., Kauschke, S.G., Eickelmann, P., Piemonti, L., Gray, N.S., Lammert, E. 2013. Pharmacological inhibition of Eph receptors enhances glucose-stimulated insulin secretion from mouse and human pancreatic islets. Diabetologia 56:1350–1355.
[69] Liu, T., Barrett, N.A., Kanaoka, Y., Yoshimoto, E., Garofalo, D., Cirka, H., Feng, C., Boyce, J.A., 2018. Type 2 Cysteinyl Leukotriene Receptors Drive IL-33-Dependent Type 2 Immunopathology and Aspirin Sensitivity. Journal of Immunology 200:915–927.
[70] Qiu, Y., Nguyen, K.D., Odegaard, J.I., Cui, X., Tian, X., Locksley, R.M., Palmiter, R.D., Chawla, A., 2014. Eosinophils and type 2 cytokine signaling in macrophages orchestrate development of functional beige fat. Cell 157:1292–1308.
[71] Fischer, K., Ruiz, H.H., Jhun, K., Finan, B., Oberlin, D.J., van der Heide, V., Kalinovich, A.V., Petrovic, N., Wolf, Y., Clemmensen, C., Shin, A.C., Divanovic, S., Brombacher, F., Glasmacher, E., Keipert, S., Jastroch, M., Nagler, J., Schramm, K.W., Medrikova, D., Collden, G., Woods, S.C., Herzig, S., Homann, D., Jung, S., Nedergaard, J., Cannon, B., Tschöp, M.H., Müller, T.D., Buettner, C., 2017. Alternatively activated macrophages do not

bioRxiv preprint doi: https://doi.org/10.1101/2020.02.21.959593; this version posted April 9, 2020. The copyright holder for this preprint (which was not certified by peer review) is the author/funder, who has granted bioRxiv a license to display the preprint in perpetuity. It is made available under aCC-BY-NC-ND 4.0 International license.

synthesize catecholamines or contribute to adipose tissue adaptive thermogenesis. Nature Medicine 23:623–630.

bioRxiv preprint doi: https://doi.org/10.1101/2020.02.21.959593; this version posted April 9, 2020. The copyright holder for this preprint (which was not certified by peer review) is the author/funder, who has granted bioRxiv a license to display the preprint in perpetuity. It is made available under aCC-BY-NC-ND 4.0 International license.

FIGURE LEGENDS

Figure 1. Characterization of subcutaneous (SC) and deep-neck (DN) progenitors. (A) Expression of 17 surface markers was determined in preadipocytes of 3 independent donors with T/C genotype for the rs1421085 locus in the FTO gene by flow cytometry. The numbers represent the percentage of positive cells. n=3 (B) Heat map visualization of 1420 differentially expressed genes (DEGs) in preadipocytes based on tissue origin; 1 to 9 labels the individual from which the sample was obtained. (C and E) Interactome maps of genes greater expressed in DN preadipocytes (C) and SC preadipocytes (E). Edges represent protein-protein interactions; 0.7 conf. (D and F) Selected significant Enriched pathways, cell components or biological processes based on DN vs SC DEGs in preadipocytes with false discovery rate (FDR) values; Italic font: pathway also appears after differentiation (D) higher expressed in DN (F) and in SC preadipocytes; n=9 donors, 6 samples/donor.

Figure 2. The degree of differentiation and browning of subcutaneous (SC) and deep-neck (DN) adipocytes. (A) Ratio of differentiated adipocytes over the total number of cells. (B) Heat map displaying the expression profiles of general adipocyte marker genes. (C) Texture sum variance and median Ucp1 protein content of adipocytes (as compared to SC white adipocytes) per cell. In every experiment, 2000 cells per each sample were recorded and measured. (D) Based on the raw gene-expression data the browning probability of the samples was analyzed and visualized by ProFAT software. (E) Browning probability considering tissue origin and differentiation protocol. (F) Expression profile of BATLAS marker genes in SC and DN adipose progenitors and differentiated samples. (G) Estimation of brown cell percentage by BATLAS considering tissue origin and differentiation protocol, n=9 donor, 4 samples/donor. (H) Expression of UCP1 in adipocyte lysates of one representative donor detected by immunoblotting. Densitometry of immunoblots was performed with samples of three independent donors. W: white differentiation protocol; B: brown differentiation protocol. 1 to 9 labels the individual from which the sample was obtained. In the comparison of two groups, paired two-tailed Student's t-test, in multi-factor comparison, two-way ANOVA and post hoc Tukey's test was used, *$p<0.05$, **$p<0.01$.

Figure 3. Differentially expressed genes (DEGs) in subcutaneous (SC) and deep-neck (DN) mature adipocytes. (A) Heat map shows the expression profile of 1049 DEGs in SC and DN mature adipocytes. Based on how these DEGs are expressed in preadipocytes, four distinct groups were formed (Group 1-4). 1 to 9 labels the individual from which the sample was obtained. (B) Venn diagram shows the DEG numbers based on DN and SC comparison at preadipocyte and differentiated adipocyte state. (C) Interactome map and (D) Selected Significantly Enriched pathways and their false discovery rate (FDR) value based on DN vs SC DEGs in Group 1; 0.4 conf. (E) Interactome map and (F) Selected significantly Enriched pathways and their FDR values in Group 2; 0.4 conf. Edges represent protein-protein interactions. Italic font: pathway also appears in preadipocyte state; Capital letters: Pathway also appears in FTO obesity-risk allele based comparison. W: white differentiation protocol; B: brown differentiation protocol.

Figure 4. Interactome maps and enriched pathways, biological processes or cellular components expressed lower in deep-neck (DN) as compared to subcutaneous (SC) adipocytes. Groups of genes were defined in Figure 3A. (A) Interactome map and (B) Selected Significantly Enriched pathways and their false discovery rate (FDR) values based on DN vs SC differentially expressed genes in Group 3; 0.4 conf. (C) Interactome map and (D) Selected significantly Enriched pathways and their FDR values in Group 4; 0.4 conf.

bioRxiv preprint doi: https://doi.org/10.1101/2020.02.21.959593; this version posted April 9, 2020. The copyright holder for this preprint (which was not certified by peer review) is the author/funder, who has granted bioRxiv a license to display the preprint in perpetuity. It is made available under aCC-BY-NC-ND 4.0 International license.

Edges represent protein-protein interactions. Italic font: pathway also appears in preadipocyte state; Capital letters: Pathway also appears in FTO obesity-risk allele based comparison.

Figure 5. Expression of genes up- and downregulated after browning protocol in both subcutaneous (SC) and deep-neck (DN) adipocytes. (A) Heat map of the upregulated genes. 1 to 9 labels the individual from which the sample was obtained. (B and E) Venn diagrams of the number of genes responding to brown differentiation. (C and F) Representation of overlapping up- and downregulated genes, respectively, in a Gephi interactome map where the size of circles is proportional to the fold change in expression values. (D) Expression profile of *KLF11* based on DESeq normalized RNAseq data, statistics: GLM ***$p<0.001$. PA: preadipocytes, W: white differentiation protocol, B: brown differentiation protocol.

Figure 6. Gene expression analyses based on the presence of FTO obesity-risk allele. (A) Heat map shows the expression profile of marker genes from ProFAT database. (B) Heat map visualization shows differences of brown marker genes based on BATLAS database; samples ordered; n=6. (C) Heat map shows the expression profile of differentially expressed genes (DEGs) based on the presence of FTO obesity-risk alleles in SC and DN adipose progenitors and differentiated samples. (D and E) Interactome map and selected significantly enriched pathways, biological processes or cell components and their false discovery rate (FDR) values of lower expressed genes in FTO obesity-risk allele carrier samples, 0.7 conf (F and G). Interactome map and selected significantly enriched pathways, biological processes or cell components and their FDR values of higher expressed genes in FTO obesity-risk allele carrier samples. Edges represent protein-protein interactions. SC: subcutaneous DN: deep-neck, W: white differentiation protocol; B: brown differentiation protocol. (H and I) Interactome map and Significantly enriched pathways with their FDR values of ProFAT browning marker genes; 0.4 conf. (J and K) Interactome map and Significantly enriched pathways with their FDR values of BATLAS browning marker genes; 0.4 conf. Italic font: pathway also appears in preadipocyte state; Capital letters: Pathway also appears in FTO obesity-risk allele based comparison. (L) FTO genotype affected genes among the DEGs in DN and SC samples. 1 to 9 labels the individual from which the sample was obtained.

bioRxiv preprint doi: https://doi.org/10.1101/2020.02.21.959593; this version posted April 9, 2020. The copyright holder for this preprint (which was not certified by peer review) is the author/funder, who has granted bioRxiv a license to display the preprint in perpetuity. It is made available under aCC-BY-NC-ND 4.0 International license.

Table 1A.

Gene	BC score	Bridges	FC	Gene Description
ESR1	1445	3	2.0	estrogen receptor 1
UCP1	1323	1	6.1	uncoupling protein 1 (mitochondrial, proton carrier)
MT2A	1061	2	2.4	metallothionein 2A
LEPR	988	1	1.9	leptin receptor
IFIH1	957	0	2.0	interferon induced with helicase C domain 1
IRF7	880	2	2.0	interferon regulatory factor 7
NLRC4	864	1	1.9	NLR family, CARD domain containing 4
CTSL	813	1	1.9	cathepsin L
AGT	745	2	2.4	angiotensinogen (serpin peptidase inhibitor, clade A, member 8)
MAPK10	720	2	1.8	mitogen-activated protein kinase 10

Table 1B.

Gene	BC score	Bridges	FC	Gene Description
BMP4	2776	8	3.1	bone morphogenetic protein 4
CD34	2048	3	3.6	stem cell adhesion
EFNA5	1519	1	2.2	ephrin-A5
RARB	1362	0	3.9	retinoic acid receptor, beta
ALDH1A3	1194	1	4.4	aldehyde dehydrogenase 1 family, member A3
SMOC1	1138	1	3.2	SPARC related modular calcium binding 1
TBX1	1125	3	2.5	T-box 1
RELN	1087	0	3.1	reelin
SEMA3B	1050	1	2.2	immunoglobulin domain (semaphorin) short basic domain, secreted, 3B
SPTA1	1046	1	2.1	spectrin, alpha, erythrocytic 1 (elliptocytosis 2)

Table 1. Betweenness centrality (BC) score and Bridges number identified based on STRING Interactome network analysis by Igrapg R and Fold Changes (FC) identified by DESeq in R of the differentially expressed genes DN vs SC comparison. Average FC when two data were considered. (A) Table shows genes/proteins from Group 1; (B) Table shows genes/proteins from Group 2. n = 9 donors

bioRxiv preprint doi: https://doi.org/10.1101/2020.02.21.959593; this version posted April 9, 2020. The copyright holder for this preprint (which was not certified by peer review) is the author/funder, who has granted bioRxiv a license to display the preprint in perpetuity. It is made available under aCC-BY-NC-ND 4.0 International license.

Table 2A.

Gene	BC score	Bridges	FC	Gene Description
COL1A1	2057	4	2.1	collagen, type I, alpha 1
GPC3	1113	1	3.0	glypican 3
KRT7	914	2	2.9	keratin 7
CNR1	864	1	5.8	cannabinoid receptor 1 (brain)
THY1	822	2	2.0	Thy-1 cell surface antigen
SEMA3A	781	5	2.8	immunoglobulin domain, secreted (semaphorin) 3A
FBN2	630	2	6.4	fibrillin 2
ITGA4	617	3	2.7	integrin (antigen CD49D) alpha 4 subunit of VLA-4 receptor
KCNJ6	569	0	4.2	potassium inwardly-rectifying channel, subfamily J, member 6
KIT	543	3	7.0	v-kit Hardy-Zuckerman 4 feline sarcoma viral oncogene homolog

Table 2B.

Gene	BC score	Bridges	FC	Gene Description
POSTN	1541	5	5.8	periostin, osteoblast specific factor
RUNX2	1454	5	2.9	runt-related transcription factor 2
NCAM1	1230	4	3.4	neural cell adhesion molecule 1
GATA2	1050	3	3.5	GATA binding protein 2
EDIL3	901	3	4.6	EGF-like repeats and discoidin I-like domains 3
PAX3	840	4	87.1	paired box 3
IRX1	768	3	23.4	iroquois homeobox 1
NTNG1	760	1	7.0	netrin G1
HAND2	752	2	30.5	heart and neural crest derivatives expressed 2
ITGB2	663	2	2.6	integrin, beta 2 (complement component 3 receptor

Table 2. Betweenness centrality (BC) score and Bridges number identified based on STRING Interactome network analysis by Igrapg R and Fold Changes (FC) identified by DESeq R of the differentially expressed genes DN vs SC comparison. Average FC when two data were considered. (A) Table shows genes/proteins from Group 3; (B) table shows genes/proteins from Group 4. n = 9 donors

was not certified by peer review) is the author/funder, who has granted bioRxiv a license to display the preprint in perpetuity. It is made available under aCC-BY-NC-ND 4.0 International license.

A

Surface antigene expression

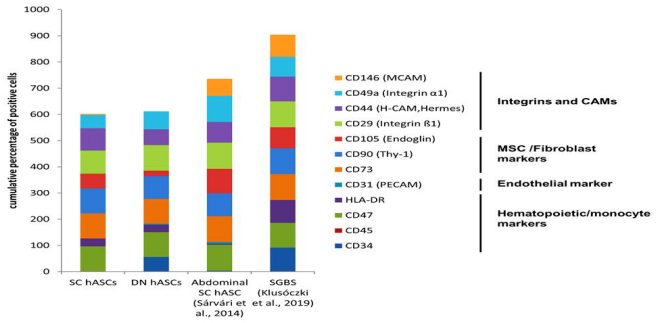

B

DEGs in SC and DN preadipocytes

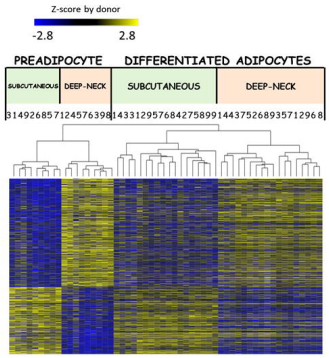

C

Interactome of higher expressed genes in DN as compared to SC preadipocytes

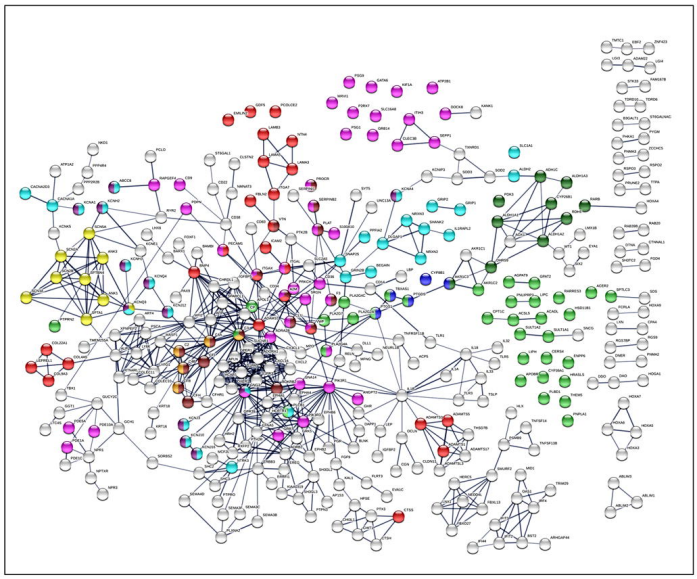

D

Enriched pathways, biological processes or components	FDR
Complement and coagulation cascades	**7.84e-0.6**
Signaling by Retinoic Acid	**0.0036**
Interaction between L1 and Ankyrins	**0.0036**
Activation of C3 and C5	**0.0053**
Extracellular matrix organization	**0.0097**
Neuronal System	**0.0115**
Hemostasis	**0.0160**
Lipid metabolism	**0.0349**
Synthesis of Prostaglandins (PG) and Thromboxanes (TX)	**0.0410**
Potassium Channels	**0.0410**

E

Interactome of lower expressed genes in DN as compared to SC preadipocytes

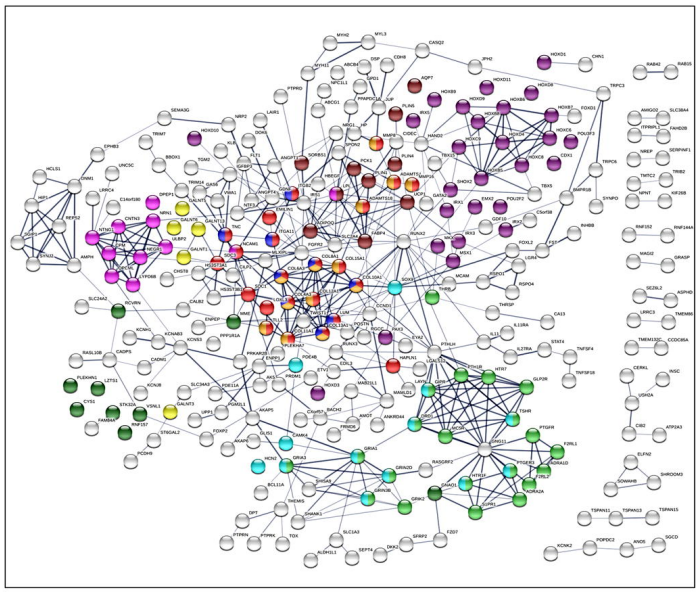

F

Enriched pathways, biological processes or components	FDR
Transcription regulation by proteins containing Homeobox/Homedomain	**1.84e-0.9**
Neuroactive ligand-receptor interaction	**0.00035**
Extracellular matrix organization	**0.00036**
PPAR signaling pathway	**0.0011**
Degradation of the extracellular matrix	**0.0046**
Post-translational modification: synthesis of GPI-anchored proteins	**0.0067**
Integrin cell surface interactions	**0.0134**
Myristate	**0.0376**
cAMP signaling pathway	**0.0411**
Mucin type O-glycan biosynthesis	**0.0439**

was not certified by peer review) is the author/funder, who has granted bioRxiv a license to display the preprint in perpetuity. It is made available under aCC-BY-NC-ND 4.0 International license.

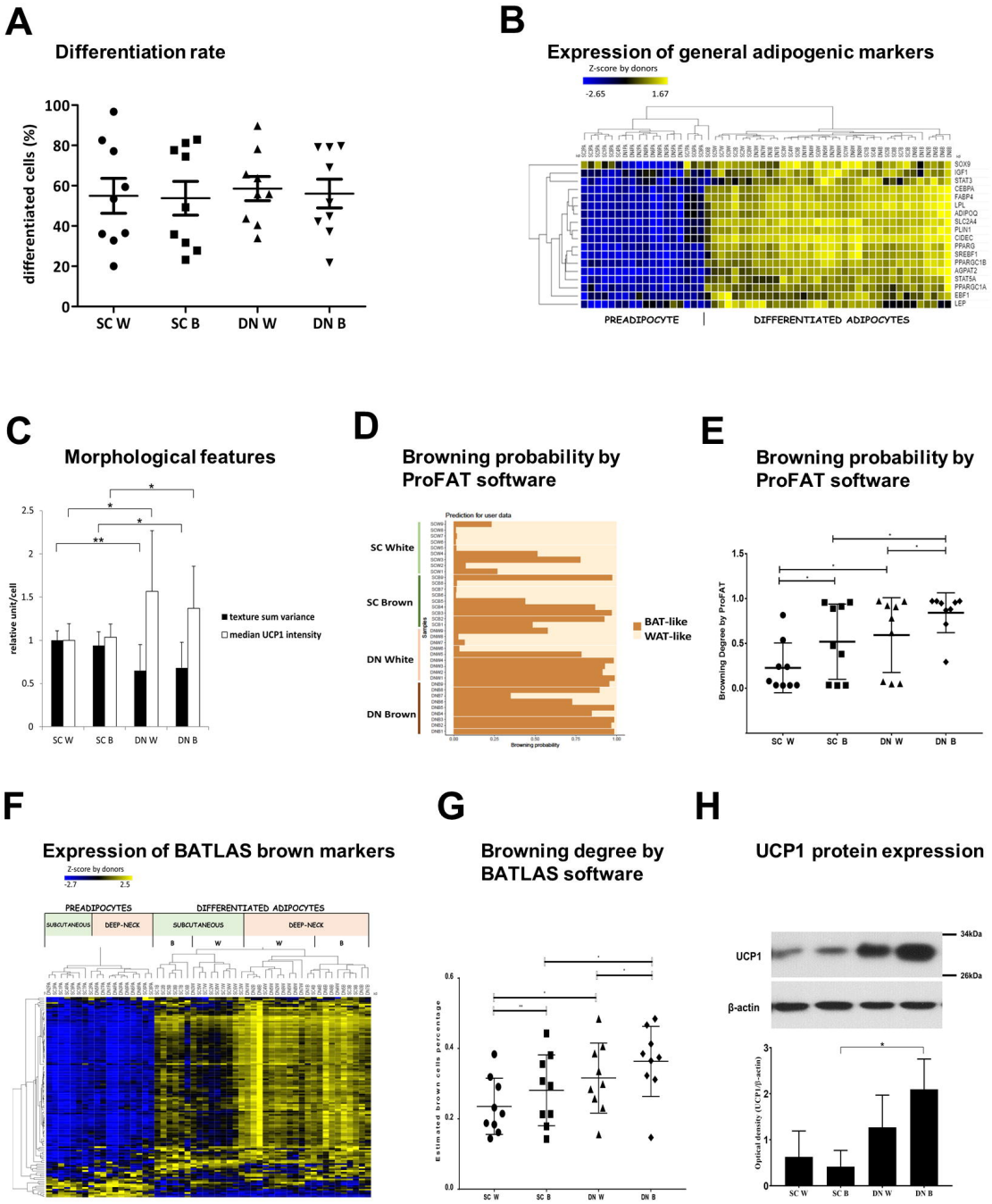

was not certified by peer review) is the author/funder, who has granted bioRxiv a license to display the preprint in perpetuity. It is made available under aCC-BY-NC-ND 4.0 International license.

A

DEGs in SC and DN adipocytes

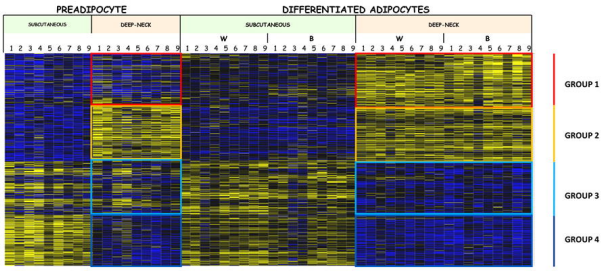

B

DEG numbers in DN adipocytes comparing with SC samples

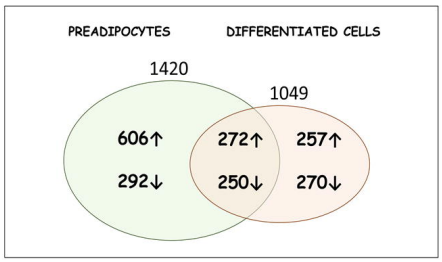

C

Interactome of Group 1 genes

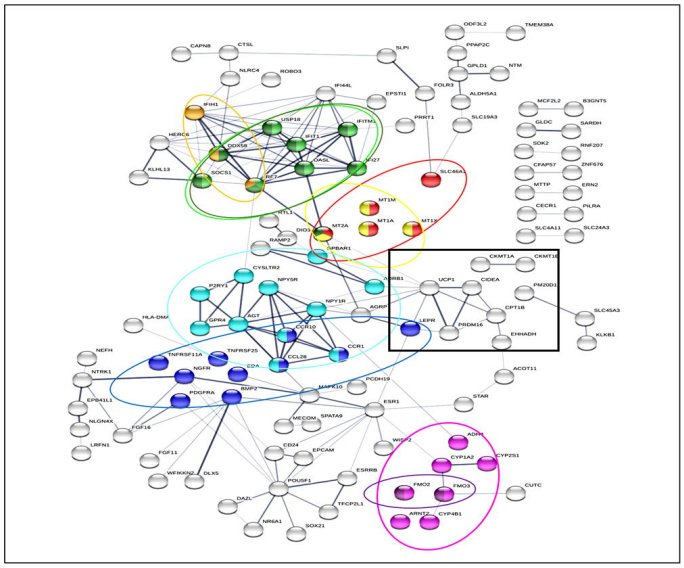

D

Enriched pathways, biological processes or components	FDR
Interferon alpha/beta signaling	0.0031
Metallothioneins bind metals	0.0031
Phase I - Functionalization of compounds	0.0126
Interferon Signaling	0.0129
Class A/1 (Rhodopsin-like receptors)	0.0251
TRAF3-dependent IRF activation pathway	0.0337
Mineral absorption	0.0427
Cytokine-cytokine receptor interaction	0.0427
FMO oxidises nucleophiles	0.0482

E

Interactome of Group 2 genes

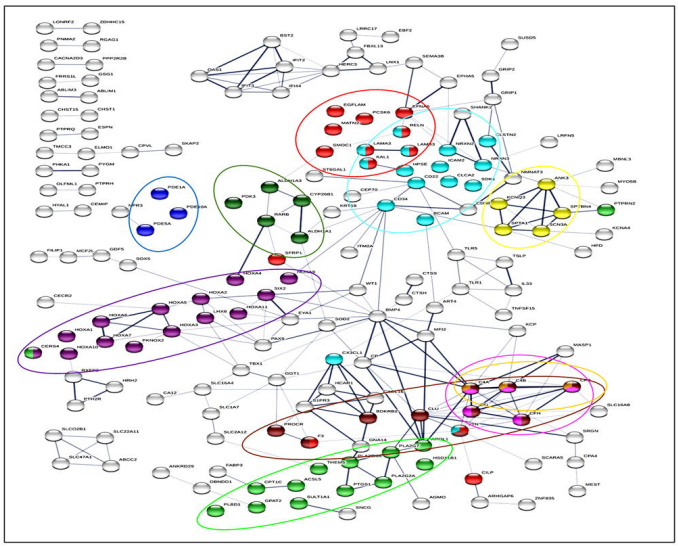

F

Enriched pathways, biological processes or components	FDR
Complement and coagulation cascades	1.22e-05
Transcription regulation by proteins contain Homeobox/Homedomain	8.80e-05
Extracellular matrix	0.0025
Cell adhesion	0.006
Interaction between L1 and Ankyrins	0.007
Lipid metabolism	0.016
Activation of C3 and C5	0.016
SIGNALING BY RETINOIC ACID	0.017
Staphylococcus aureus infection	0.039
cGMP degradation by PDEs	0.040

was not certified by peer review) is the author/funder, who has granted bioRxiv a license to display the preprint in perpetuity. It is made available under aCC-BY-NC-ND 4.0 International license.

A

Interactome of Group 3 genes

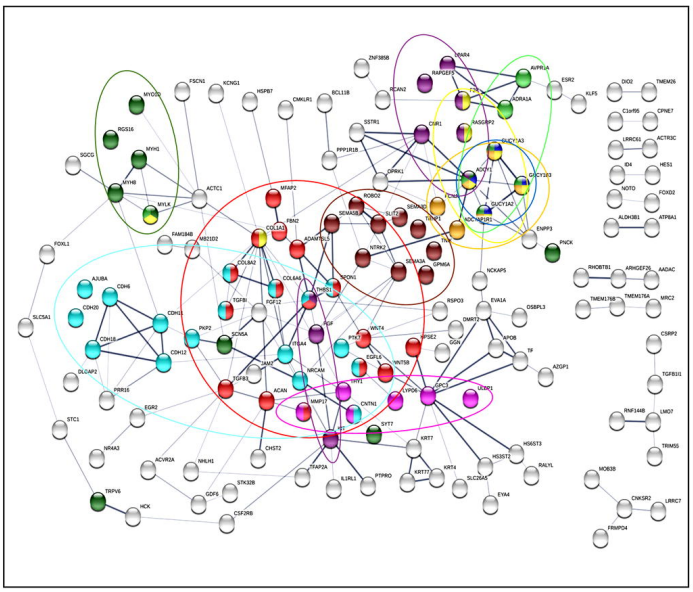

B

Enriched pathways, biological processes or components	FDR
Extracellular matrix	4.15e-06
CELL ADHESION	0.00087
Calmodulin binding	0.0189
guanylate cyclase activity	0.0189
PLATELET ACTIVATION	0.0129
Circadian entrainment	0.0325
Vascular smooth muscle contraction	0.0325
RAP1 SIGNALING PATHWAY	0.0325
Neurogenesis	0.0320
Synthesis of GPI-anchored proteins	0.0419

C

Interactome of Group 4 genes

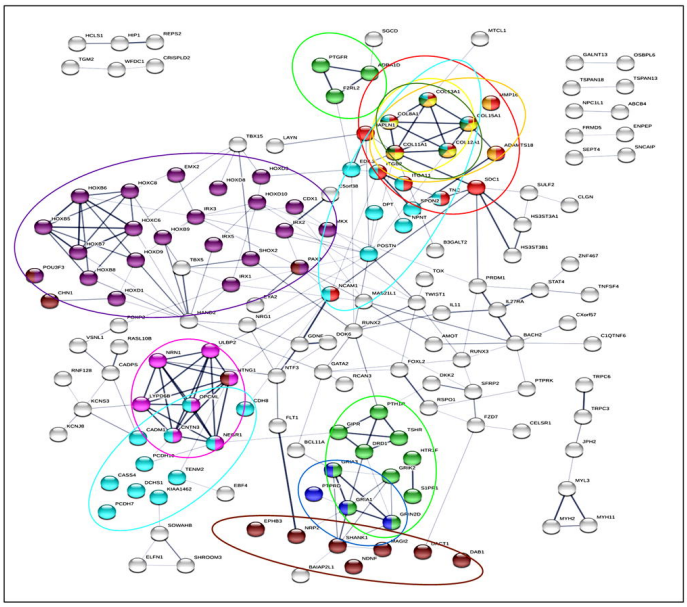

D

Enriched pathways, biological processes or components	FDR
Transcription regulation by proteins contain Homeobox/Homedomain	4.80e-12
CELL ADHESION	1.93e-08
Neuroactive ligand-receptor interaction	0.0010
Neurogenesis	0.0024
EXTRACELLULAR MATRIX ORGANISATION	0.0072
Synthesis of GPI-anchored proteins	0.0123
Collagen chain trimerization	0.0128
Synaptic adhesion-like molecules	0.0128
Degradation of the extracellular matrix	0.0481
Collagen degradation	0.0481

was not certified by peer review) is the author/funder, who has granted bioRxiv a license to display the preprint in perpetuity. It is made available under aCC-BY-NC-ND 4.0 International license.

A

80 DEGs comparing brown vs white protocols

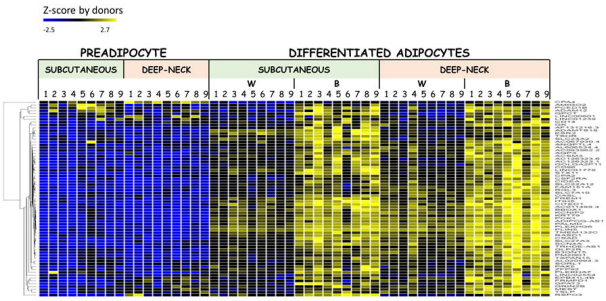

B

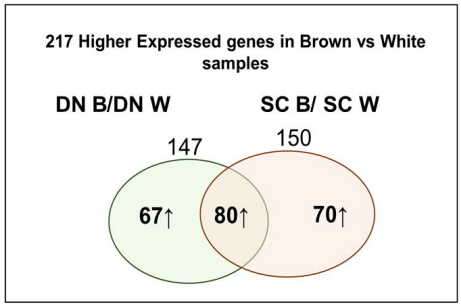

C

Interactome of 80 genes upregulated after brown protocol

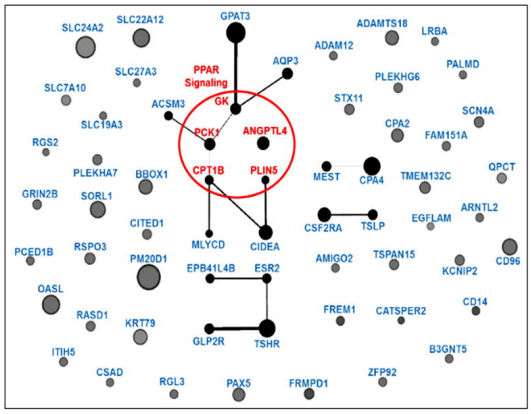

D

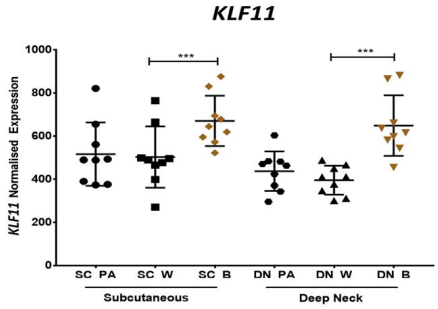

E

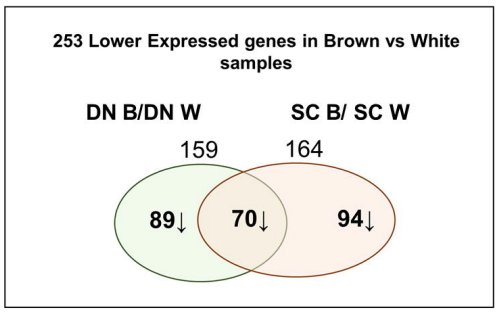

F

Interactome of 70 genes downregulated after brown protocol

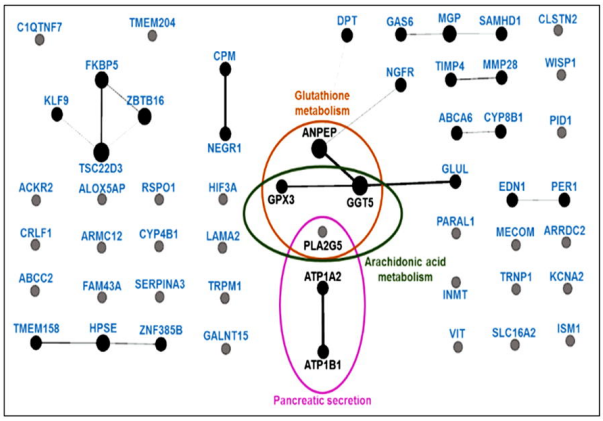

was not certified by peer review) is the author/funder, who has granted bioRxiv a license to display the preprint in perpetuity. It is made available under aCC-BY-NC-ND 4.0 International license.

A

Brown markers from ProFAT database

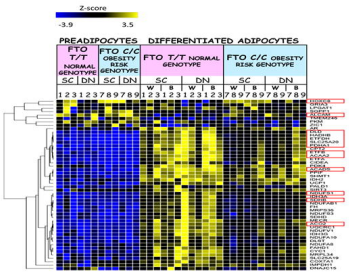

B

Brown markers from BATLAS database

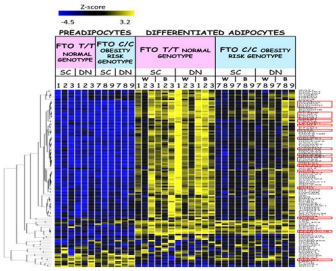

C

1295 DEGs based on the presence of *FTO* obesity-risk allele

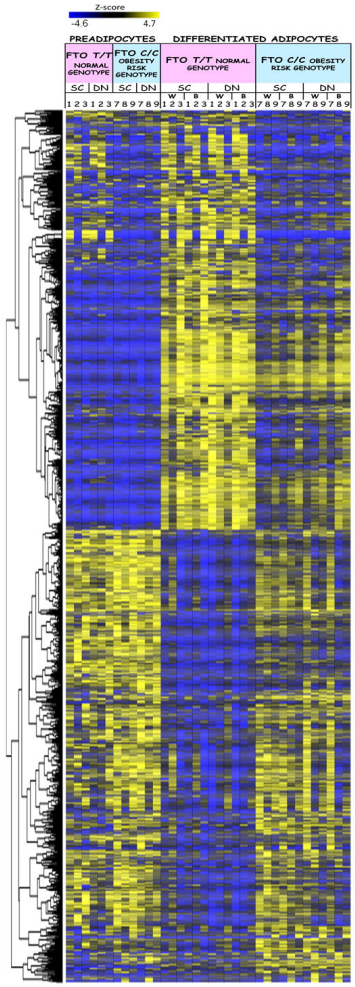

D

Interactome of less expressed genes in *FTO* obesity-risk samples

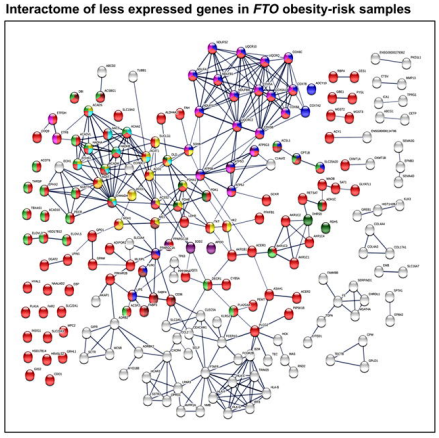

E

Enriched pathways	FDR
Metabolic Pathways	4.47e-28
Fatty acid metabolism	1.15e-13
Thermogenesis	3.88e-11
Respiratory electron transport	4.42e-11
Carbon metabolism	3.96e-10
Valin, leucine and isoleucine degradation	2.3e-06
PPAR signaling	7.01e-06
SIGNALING BY RETINOID ACID	3.49e-05
Glyoxalate and Dicarboxilate metabolism	0.00043
Mitochondrial biogenesis	0.0045

F

Interactome of higher expressed genes in *FTO* obesity-risk samples

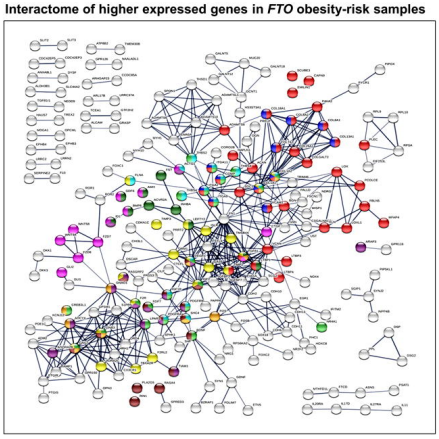

G

Enriched pathways	FDR
EXTRACELLULAR MATRIX ORGANISATION	4.5e-10
Integrin cell surface interaction	0.0007
PLATELET ACTIVATION, SIGNALING AND AGGREGATION	0.002
Focal adhesion	0.027
TGF-beta signaling pathway	0.027
PI3-Akt signaling pathway	0.027
RAP1 SIGNALING PATHWAY	0.027
Relaxin signaling pathway	0.036
Hippo signaling pathway	0.036
Ras signaling pathway	0.044

L

DEG numbers based on FTO obesity-risk allele presence and tissue origin

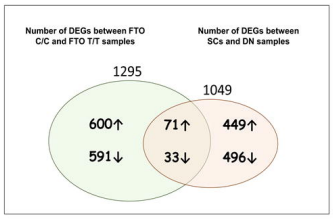

H

Brown marker genes from ProFAT database

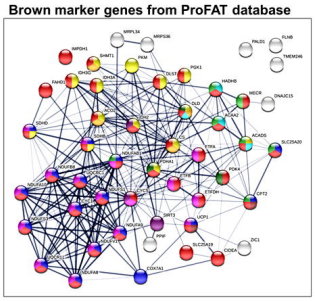

I

Enriched pathways	FDR
Metabolic Pathways	3.06e-27
Respiratory electron transport	3.73e-25
Thermogenesis	2.69e-19
Carbon metabolism	1.24e-18
Fatty acid metabolism	3.16e-06
Glyoxalate and Dicarboxilate metabolism	5.73e-06
Valin, leucine and isoleucine degradation	3.64e-05
Signaling by Retionic Acid	0.0011
Transcriptional activation of mitochondrial biogenesis	0.0018
PPAR sygnaling pathway	0.0419

J

Brown marker genes from BATLAS database

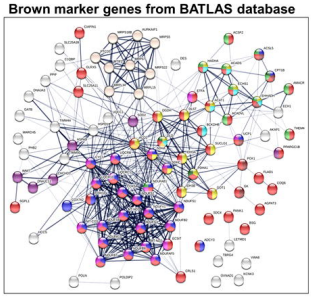

K

Enriched pathways	FDR
Metabolic Pathways	5.96e-33
Respiratory electron transport	2.20e-28
Thermogenesis	7.54e-27
Carbon metabolism	6.02e-17
Mitochondrial translation initiation	3.35e-08
Fatty acid metabolism	4.08e-08
Valin, leucine and isoleucine degradation	8.86e-08
Glyoxalate and Dicarboxilate metabolism	4.70e-07
PPAR signaling Pathway	1.70e-05
Mitochondrial biogenesis	0.00011
Signaling by Retinoid Acid	0.011